An-Najah National University

Faculty of Graduate Studies

INVESTIGATION OF THE RADIATION BEHAVIOUR OF FLUOROAPATITE CRYSTALS AS MATRICES FOR NUCLEAR WASTE IMMOBILIZATION

By

Rand Ghassan Hazzam

Supervisors

Dr. Mohammed Suleiman

Prof. Frederico Garrido

This Thesis is Submitted in Partial Fulfilment of the Requirements for the Degree of Master of Chemistry, Faculty of Graduate Studies, An-Najah National University, Nablus, Palestine.

2023

INVESTIGATION OF THE RADIATION BEHAVIOUR OF FLUOROAPATITE CRYSTALS AS MATRICES FOR NUCLEAR WASTE IMMOBILIZATION

By

Rand Ghassan Hazzam

This Thesis was Defended Successfully on 19/1/2023 and approved by

Dr. Mohammed Suleiman Supervisor	Signature
Prof. Frederico Grrido Co-Supervisor	Signature
Dr. Muayad Abusaa External Examiner	Signature
Dr. Diaa Aref Internal Examiner	Signature

Dedication

I dedicate my work to my inspiration my father soul, to my role model in this life my mother (Dr. Samar Al-Shakhshir), to my backbones Lana, Nedal and my twin Rola.

To all professors and doctors that taught me any word and to all people that gave me an opportunity and believe in me, to my friends and to everyone that had a mark and passed in my educational life, and finally to the purest souls around me.

Acknowledgments

First of all, I would like to thank Allah for everything.

I would like to thank an-Najah National University, which opened its doors for student exchange by Erasmus+ program to do my thesis research at Paris Saclay University.

I would like to thank the University of Paris Saclay especially IJClab for making me part of their team.

I also extend my heartfelt gratitude to my supervisor the director of energy and environment lab at IJClab Prof. Frederico Garrido for his help, encouragement and guidance throughout my research work. I would like also to thank my supervisor Dr. Mohammed Suliman for his guidance, encouragement and motivation.

Also I would like to thank my group at IJClab for their help, support and motivation throughout my work especially dee jay Cerico.

My special thanks for Dr. Ahmad Basalat and Dr. Hadil Abu Alrub for giving me this opportunity to be part of their great family in France.

Great thanks are extended to the technical stuff at the SCALP facility in the chemistry lab in energy & environment lab at IJClab Florian Pallier, Jérôme Bourçois and Silvin Hervé for their technical help.

Special thanks extended to my mother Dr. Samar Al-Shakhshir for help, motivation and support also special thanks to Eng. Lana, Nedal and Rola for motivation, help and support.

Also I would like to thank Dr. Ahed Zyoud for his support.

I would like to extend my thanks to Mrs. Nisreen Hamadneh for her help.

Rand G. Hazzam

Declaration

I, the undersigned, declare that I submitted the thesis entitled:

INVESTIGATION OF THE RADIATION BEHAVIOUR OF FLUOROAPATITE CRYSTALS AS MATRICES FOR NUCLEAR WASTE IMMOBILIZATION

I declare that the work provided in this thesis, unless otherwise referenced, is the researcher's own work, and has not been submitted elsewhere for any other degree or qualification.

Student's Name: Rand Ghassan Hazzam

Signature: Rand

Date: 19/1/2023

List of Contents

List of Tables

List of Figures

List of Schemes

List of Appendices

INVESTIGATION OF THE RADIATION BEHAVIOUR OF FLUOROAPATITE CRYSTALS AS MATRICES FOR NUCLEAR WASTE IMMOBILIZATION

By
Rand Ghassan Hazzam
Supervisors
Dr. Mohammed Suleiman
Prof. Frederico Garrido

Abstract

The increasing generation of radioactive waste from economic applications and radioactive elements presents a significant challenge in terms of safe disposal and storage. Fluorapatite crystals have been proposed as a potential solution for nuclear waste immobilization due to their ability to form a solid and insoluble matrix that can effectively contain radioactive elements. However, as a relatively new technology, further research is required to fully evaluate its long-term effectiveness and safety.

Aim: This research aims to understand the effect of radiation induced by the decay of actinides in fluorapatite crystals ($Ca_5(PO_4)_3F$), and to investigate the crystalline defects in natural apatite and their healing rates. Additionally, it is aimed to determine whether apatite can be used as a potential alternative matrix for embedding high-level radioactive waste (HLW), such as fission products and minor actinides, currently stored in nuclear glasses.

Methods: An ex-situ ion implantation technique was used in this study, where pre-prepared natural fluoroapatite crystals ($Ca_5(PO_4)_3F$), sourced from the Durango mine in Mexico, were implanted with 500 keV Bi^{3+} (heavy-ions) at the JANNuS facility located at IJCLab to simulate the decay of actinides. Different fluences ranging from 10^{12} to 10^{14} cm^{-2} were applied at different temperatures especially at room temperature and at 100 °C. The samples were then characterized using Rutherford backscattering spectroscopy/channeling (RBS/C) on the Ion Beam Analysis (IBA) beam line of the platform using 1.4 MeV He^{+} ions in channeling conditions. The RBS spectra data were simulated by using Mont Carlo simulations (McChasy RBS/C code). This adopted approach allows for a comprehensive analysis of the structural and compositional properties of the apatite crystals before and after irradiation, providing insight into the effects of heavy recoil nuclei and the simulation of actinide decay. Transmission electron microscope (TEM) was employed to monitor the evolution of damage induced by Bi^{3+} ions.

Results: The RBS spectra data simulated by using Mont Carlo simulations (McChasy code) clarified the damage formation in the crystal induced by bombarding with Bi^{3+} ions, at different fluences. The damage distribution and its kinetics were extracted from RBS/C experiments and compared to transmission electron microscope (TEM) images to monitor the evolution of damage induced by Bi^{3+} ions, which deduced the presence of amorphous

regions in apatite single crystals, supporting the main idea that apatite can be used as an alternative matrix for embedding HLW.

Conclusions: The effect of radiation of alpha decay of actinides, on the crystalline structure of natural fluorapatite crystals $Ca_5(PO_4)_3F$ was studied using Bi^{3+} ions as a model of recoil nuclei. The ex-situ RBS/C technique was used to characterize 500 keV Bi implanted crystals at increasing ion fluence, simulating the effect of the damage generated by heavy recoil nuclei. The Monte Carlo McChasy code simulation fits very satisfactorily the Rutherford Backscattering by channeling mode experimental results. As the ion fluence increases the amount of damage that was modelled as RDA (Randomly Displaced Atoms) up to the final amorphization of the crystal at a fluence in the range 10^{14} cm^{-2}. TEM characterization showed that the induced defects for the selected apatite samples increase with the increase in ion fluence, this is in accordance with RBS/C results.

Keywords: Fluoroapatite crystals; Rutherford backscattering spectroscopy/channeling (RBS/C); ex-situ RBS/C; Monte Carlo simulation McChasy code; high level waste (HLW); Bi^{3+} ions.

Chapter One
Introduction

1.1 Types of Nuclear Waste

Nuclear materials are a class of solids that must face extreme environment in terms of radiation sources and possible other extreme thermodynamic conditions (temperature, pressure, chemical agents). Depending on their role in a nuclear facility (e.g., nuclear fuels, steels from the reactor vessel, nuclear waste matrices) nuclear materials are submitted to various irradiation sources that make difficult the study of their properties towards irradiation, as for instance their radiation stability or the capability to confine incorporated chemical elements. A key problem with nuclear power is what to do with the waste products when the fuel is completely spent since it is no longer useful in power generation. This waste is still very unsafe if not stored correctly [1, 2]. One way to reduce its hazardous relies on the use of nuclear waste immobilization that is the conversion of waste into a specific nuclear waste form by several processes. The main strategies to manage the spent nuclear fuel are the following ones: firstly, to store the fuel without treatment: direct disposal of the spent fuel in an underground geological site. Secondly, is the reprocessing of the spent nuclear: dissolution of the fuel in nitric acid, separation of Uranium (U) and Plutonium (Pu) from the remaining part (fission products and minors actinides). France [2] is currently using this approach and the wastes (fission products and minors actinides) are embedded into a glass (borosilicate glass) before final disposal in an underground facility.

Immobilization of waste is accomplished by its chemical incorporation into the structure of a suitable matrix (typically cement, glass, or ceramic) [3]. It is therefore trapped into the structure and can hardly escape (the diffusion of a chemical specie in the solid is very slow and it is expected that a possible release will take place at geological times and therefore without radioactivity of wastes). Nuclear wastes are classified into three categories based on their radioactivity: very low and low, intermediate, and high.

Very Low Level Wastes (VLLW) do not require any additional safety precautions under the current rule because their radioactivity levels are so low. Since they do not need special management, these wastes are typically transferred to civil landfills or burned along household waste. [4]. Low Level Wastes (LLW) are those that are deemed to have low α content and some β/γ content. LLW includes waste produced when radioactive

materials are used in industry, medicine, and research. LLW often comprises of discarded safety clothing, equipment, and building rubble from nuclear host sites [4]. It normally does not need shielding, but containment is necessary to prevent any direct handling. Since 1959, the majority of the UK's solid LLW has been disposed of at facilities in Drigg, Cumbria, or Dounreay, Scotland, that are approved by the United Kingdom Atomic Energy Authority (UKAEA) [5].

Materials that have been exposed to radiation in a nuclear reactor, as well as equipment from the reprocessing of radioactive materials and chemical residues, make up the majority of Intermediate Level Wastes (ILWs). The term "ILW" refers to radioactive wastes whose activity is higher than that of LLW materials but not high enough to fall under the high-level category. The restriction specifically says that the waste cannot self-heat radiologically [5]. ILWs are frequently held at the reactor sites where they are produced as a byproduct of both civil and military nuclear operations, as well as in reprocessing and navy dockyards. Reactor parts, filters, chemical residues, fragments of radioactive fuel covering, and items polluted with plutonium can all be found in ILWs [5].

High-level waste (HLW), often known as highly radioactive waste, mostly takes two types. One is the fuel that was left over after being utilized to produce electricity in nuclear power reactors. The other is waste created by factories that manufacture nuclear weapons or by factories that reprocess and recycle old fuel from power plant [6, 7].

High radiation levels are, of course, a defining characteristic of high-level waste, but the thing that makes it stand out most is certainly the fact that it needs particular handling and considerations, such substantial biological shielding and engineered cooling systems due to the radiodecay heat load. The phrase "high-level waste" typically refers to the liquid effluent known as raffinate that is produced during the first cycle of fuel reprocessing operations to recover plutonium and unburned uranium. Unless they are removed from the waste, the actinides are included in any matrix that has a high enough concentration of fission products to require cooling (the alpha-emitting transuranium elements) [8].

Other examples of what is sometimes considered as high-level waste include a container containing millions of curies of the gaseous fission product krypton-85 and highly radioactive reactor parts that have been removed, such as control rods, piping, or flow orifices[8].

The most problematic waste, referred to as "high level" nuclear waste (HLW), is highly radioactive, has an extremely long half-life and requires cooling due to the nuclei decay, which gives off heat and radiation[2]. Chemical immobilization is commonly used in the consistent treatment of HLW [3].

Chemically and thermally stable materials are required for the immobilization of high-level radioactive α-emitters in a deep geological repository across geologic timescales. One of the most important variables to examine is the material's radiation behavior. When a crystalline to amorphous change occurs, radiation can have a significant impact on chemical durability by modifying atomic bonds [9].

Large volumes (tens of millions of cubic meters), high total activity (billions of Curies), and highly diverse and complex compositions characterize high-level nuclear waste in the United States. The three main sources of nuclear waste are spent nuclear fuel from commercial and research reactors, liquid waste created during commercial spent nuclear fuel reprocessing, and waste generated by nuclear weapons and naval propulsion programs. From the dismantling of nuclear weapons, over 100 metric tons of plutonium and hundreds of tons of highly enriched uranium have been added to the latter category [10].

For permanent disposal, most of these wastes will require chemical treatment, processing, and solidification into waste forms. The long-term effects of radiation on waste form solids are a major concern in the long-term containment strategy's performance evaluation. The radiation dose from the reactor neutron irradiation is already large in the case of spent nuclear fuel, and extra damage accumulated during disposal is not expected to be significant. Post-disposal radiation damage to waste form glasses and crystalline ceramics, on the other hand, is significant [10].

The proper containment and management of radioactive waste is essential for the safe use of nuclear power. Delay and decay, dilute and scatter, or concentrate and contain are the most popular waste management approaches, with the latter being most suited for the long-lived nuclides found in high-level waste (HLW) [11].

For radioactive waste immobilization “concerning long-term disposal, a chemically robust way is to immobilize the salt waste into a waste form to prevent it from dissolution and leaking into the environment”. The concentrate and contain approach demand the use of an inert host matrix. The chosen matrix should have long-term thermal, chemical, and

mechanical stability in deep geological repository conditions [12]. A suitable host must also be leach and radiation resistant, as well as able to accommodate a variety of radio nuclides in a uniform manner. Actinides (Np, Pu, Am, Cm), which have the longest half-lives and require storage for up to 500,000 years, are the most dangerous high-level waste elements in terms of radiotoxicity. Number of glasses, crystalline ceramic, glass-ceramic, and composite-based hosts have been proposed to meet these requirements [11].

For more hazardous waste that results from the radioactive waste treatment and conditioning process, the typical approach is to use several safety barriers. Although some forming packaging may be used, very low-level waste (VLLW) normally does not require immobilization. Cements are used for immobilization of low-level waste (LLW), although glasses provide better retention of contaminants. Glass, bitumen, cements, and geopolymers can be used to immobilize Intermediate Level Waste (ILW) with a higher hazard than LLW. LLW and ILW can be packed in safe metal and concrete containers. The most hazardous waste such as high-level waste (HLW) requires the most durable and reliable waste forms, e.g., ceramics and glasses and containers such as stainless-steel canisters for vitrified HLW and copper containers for spent nuclear fuel declared as waste [13, 14],.

Nuclear power is critical to maintaining worldwide energy growth while reducing greenhouse gas emissions. This technology must find a way to dispose of spent nuclear fuel (SNF) if it is to fulfill its potential. One possible solution is to recycle SNF while vitrifying the high-level waste (HLW). Around the world, vitrification is the preferred method for immobilizing HLW from defense and commercial fuel reprocessing. Recent advancements in recycling technology and vitrification hold considerable promise for efficiently finishing the nuclear fuel cycle in the United States [15].

For nearly 60 years, vitrification has been investigated as a way to manage HLWs following nuclear fuel reprocessing. Vitrification is one method that scientists have developed to more permanently store liquid nuclear waste. Through this procedure, the dangerous substance is changed into glass, an immobile solid that is easier to control. Glass is extremely durable and not only stops the release of hazardous species into the environment, but it also offers some protection against the release of radioactivity [10]. Almost every reprocessing country in the world has adopted the fundamental concept. However, as more experience in vitrifying a variety of wastes has been gathered,

new challenges and potential for development in waste-vitrification processes have developed. When developing solutions, the strong feedback between glass composition and process technology requires precise coordination between these two major process components [15].

Fission products, inert chemicals, and trace transuranics make up the majority of the waste stream. Nuclear waste vitrification can effectively immobilize this waste stream. Once an appropriate facility is established, the waste glass may be safely stored, transported, and disposed of. Waste vitrification is the preferred method of treating highly radioactive byproducts of SNF separations all around the world. It has become even more effective as a waste management strategy because of recent technological advancements [15]. Also, vitrification is a particularly attractive immobilization route because of the high chemical durability of the glassy product [13].

Overall, improving existing waste forms and searching for alternate matrices for immobilization of radioactive waste that have superior qualities than commercial glass-based waste forms is an essential problem connected to improving nuclear fuel cycle safety. The use of poly-phase ceramics as waste hosts/matrices is one of the most often promoted solutions. Hatch was the first to propose the use of ceramics for radwaste immobilization in early 1953. When compared to borosilicate glasses, there are various ceramic phases that have better chemical endurance. A particular a kind of Synthetic Rock (SYNROC10, Titanate-based ceramics) is stable in moist conditions above 300°C, whereas borosilicate glass has poor chemical stability even at temperatures below 100°C [11].

It is not easy to find a suitable wasteform (matrix) for nuclear waste immobilization, and durability is not the only factor to consider. The most important criteria, which are reliable, simple, and rugged technologies and equipment, may have advantages over complex or sensitive equipment and processes. Immobilization can be accomplished using a variety of matrix materials and techniques. The two main factors are the capability of the matrix to confine foreign elements (diffusion of that element must be as slow as possible; very low diffusion coefficient) and the radiation tolerance of the matrix. The choice of the immobilization technology depends on the physical and chemical nature of the waste and the acceptance criteria for the storage and disposal facility to which the waste will be sent [3].

Cementation and vitrification are the main commercially accessible and proven feasible immobilization technologies, but bitumen and polymeric materials are utilized to a smaller extent, and ceramification is a future technology [3]. Furthermore, borosilicate and aluminophosphate glasses are the two most common forms of glass used to immobilize nuclear wastes. Both materials allow high waste loadings and can immobilize large amounts of actinides. Borosilicate glasses can accommodate up to 7.2 mass pct of PuO_2 for example [2].

The key issue during production of vitreous wasteforms is to balance the waste loading (to minimize volume), viscosity (ease of pouring), volatilization (of high vapor pressure species) with waste form durability and simplicity and economics of the process. For a variety of reasons some species present in wastes including actinides, ^{99}Tc, ^{36}Cl, ^{129}I, and ^{14}C are inherently difficult to immobilize and dependent on melt pool REDuction/ OXidation (REDOX) behavior [13].

The capacity to include specific radionuclides, chemical durability, radiation-field resistance, and physical features, as well as the amount of time spent isolating waste to safeguard the environment, should all be considered in the final selection. Actinides can be incorporated into more durable crystalline ceramics, while fission products with mass numbers ranging from 85 to 106 and 125 to 147 (Kr, Sr, Y, Zr, Tc, Ru, Y, Sb, Cs, Ba, Ce, Pm, and others) can be inserted into borosilicate glass. With the development of novel fuel cycles, rising demand for safe radwaste disposal, and the expansion of nuclear power generation, particularly with advanced reactors (advanced heavy water, or fast breeder designs), the demand for new and better waste forms is only expected to grow [11].

They summarized in this article [16] the problems associated with waste ion solubility and the ensuing uncontrolled crystallization or phase separation. A controlled crystallization, resulting in a glass-ceramic, is proposed in some recent waste form designs. A review of glass and glass-ceramic systems is provided, with an emphasis on immobilizing waste components under high waste loading. Design and processing factors are discussed throughout, as well as the difference between uncontrolled undesired and controlled desirable crystallization [16].

Recent reviews of the developments in waste form research have been provided in [13]. The most recent interest has focused on developing new nuclear materials as part of new or advanced nuclear fuel cycles for future. Further research is going on to recognize

potential advanced waste form materials. On the other hand, the use of predominantly crystalline ceramic waste forms (ceramification) has been proposed, including single-phase ceramics like zircon or zirconolite to accommodate a limited range of active species like Pu, and multiphase systems like SYNROC to accommodate a broader range of active species like Pu and immobilize a maximum number of fission fragments and actinides. To date these systems have not been widely used to immobilize active waste [13].

The choice of the immobilization technology depends on the physical and chemical nature of the waste and the acceptance criteria for the long-term storage and disposal facility to which the waste will be sent. A magnitude of regulatory, process and product requirements has led to the investigation and adoption of a variety of matrices and technologies for waste immobilization. Cementation, vitrification, and ceramification are the main industrially used immobilization technologies for higher activity nuclear waste [13].

Most states that use nuclear fission for energy production have made reprocessing of nuclear waste a priority. The presence of long-lived elements in radioactive waste, such as actinides, lanthanides, and some fission products, makes handling difficult. The immobilization of these radionuclides in appropriate matrices is a critical step in the development of safe and effective geological repositories that will prevent dangerous biosphere pollution. In order to reduce the volume and the radiotoxicity of nuclear waste, several separation processes have been and continue to be investigated, aiming to recycle radiotoxic elements, such as U, Pu, Am and Cm, after their separation from the fission products [17]. In France, 1200 tones of spent fuel is generated from nuclear power plants each year, but 99.5 wt% of it is U and Pu, which is recycled for use as future energy sources. Only Am, Cm, Np, and fission products remaining after reprocessing are considered as wastes and are confined into nuclear glasses[18].

In the last decades, several single- and polyphase ceramic materials have been tested as potential nuclear waste forms for the immobilization of certain nuclear waste streams. These include separated Pu from civilian or military sources unsuitable for further use, separated minor actinides (MA = Am, Cm, Np) and separated fission products (Cs, I, Tc) from HLW concentrate. In addition to oxide-based ceramics, e. g. polyphase Synroc materials or single-phase zirconolite, perovskite, and pyrochlore ceramics, special attention has been paid to silicates like zircon ($ZrSiO_4$) and/or thorite ($ThSiO_4$) and phosphates such as monazite and apatite, beside various other phases. Specific ceramic

matrices for the immobilization of long-lived fission products such as ^{135}Cs (half-life $t_{½}$ = 3 x 10^6 years) are being developed in parallel with the development of ceramic waste forms for actinides [12]. Uranium dioxide (UO_2) is also investigated as a nuclear power plant but also as a potential nuclear waste immobilization matrix, where implantation on UO_2 with low-energy ions (Xe, La) at 773 K were performed [19]. The behavior of fluorapatite towards irradiation due to incorporated alpha-emitters was studied[20]. The single crystals of this mineral have been bombarded with 220 keV lead (Pb) ions, simulating alpha recoil nuclei, and then post irradiated with He ions. The defect concentration measured by Rutherford backscattering spectrometry (RBS) associated with channeling (RBS/C) measured the defect concentration which steadily decreases upon He-ion irradiation [20].

In a certain study [21] two different Sm- loading fluorapatite glass ceramics were successfully synthesized. The larger Sm-doped samples were affected by He irradiation while the smaller Sm-doped ones did not. The results of this study gave some ideas regarding the radiation resistance of materials in HLW management with various radionuclide loadings[21]. In another study, the polycrystalline fluorapatite $Ca_{10}(PO_4)_6F_2$ ceramic was pre-irradiated with 80 keV He+ ions to a fluence of 5 x 10^{16} ions/cm^2 at room temperature. The ceramic was made using a typical solid-state sintering technique [22]. In IJCLab the in-situ mode of RBS/C was used to investigate the accumulation of alpha recoil nuclei damage in apatite at room temperature.

The aim of this work is to investigate the radiation effects induced by the decay of actinides in fluorapatite crystals $Ca_5(PO_4)_3F$ and to study a model of creation of crystalline defects in natural apatite and its healing rates based on the chemistry of the samples and the temperature. In this framework ion beams are used with two main applications. First, energetic ion beams delivered by accelerator facilities provide an efficient way to experimentally simulate irradiation effects induced by various irradiation sources (alpha and beta decays, neutrons) by selecting the ion nature, energy, fluence, temperature during irradiation. Second, energetic ion beams are well established characterization techniques such as Ion Beam Analysis (IBA) and they well suited to provide relevant information on the material composition (depth distribution at the surface typically over a few micrometres) and on the defect content (channelling experiments on single crystals).

In the present case, the alpha radiation source will be simulated by implanting the fluoroapatite crystals with low-energy Bi ions to simulate the heavy recoil nucleus emitted during an alpha decay and using 1.4 MeV He ion irradiation at selected temperatures (room temperature RT and 100ºC) to both simulate the slowing-down of the alpha particle and to collect RBS/C spectrum in channelling geometry. The difference in defect creation at both room temperature and 100°C will be compared. To determine the radiation tolerance of irradiated natural fluorapatite from Durango, Mexico in terms of crystalline defects creation several techniques will be used which include Rutherford Backscattering Spectrometry (RBS) in channeling conditions (an ion beam analysis technique), the use of an analytical simulation software (RUMP) and Monte Carlo simulation software (SRIM and McChasy). The experimental RBS/C spectra for each type of damage will be simulated and fitted using McChasy as an ion channelling Monte Carlo simulation code. The simulation approach followed in this study is to experimentally measure and model the radiation induced damage caused by both alpha recoil nuclei and alpha particles energetic ion beams provided by accelerator facilities.

1.2 Apatite

Apatite refers to a group of phosphate minerals which includes fluoroapatite, chlorapatite, hydroxylapatite, carbonate-rich apatite, and francolite, the most common of which is fluorapatite. Because apatite can be mistaken for many other minerals, the word "apatite" comes from the Greek word "apate," which means "deceit." Green is the most common color, but it can also be blue, yellow, purple, or brown [21].

Apatite can be used as a waste form in planned nuclear waste repositories as well as in permeable reactive barriers (PRBs) to isolate groundwater radionuclides. By forming insoluble radionuclide-containing solids, phosphorus from dissolving apatite can remove a large amount of these radionuclides from solution. Apatite surfaces sorb/exchange dissolved radionuclides, especially cationic radionuclides like Sr, U, Pu, and Np, and so remove them from solution. U and Th can also be incorporated into apatite via a coupled substitution with SiO_4^{4-} and PO_4^{3-} [23].

Fluorapatite, hydroxyapatite, and chlorapatite are calcium phosphate apatites, $Ca_5(PO_4)_3(F, OH, Cl)_1$ [24], the tenth most abundant mineral on Earth and the most abundant phosphate mineral. It is the main source of phosphate for fertilizer to feed human populations, and it forms human bone and teeth. It is one of the most significant materials

to mankind for these reasons alone. Apatite is used in fluorescent lighting, phosphate detergents, as a basis material, as a geochronometer, as a gemstone, and as a laser material. With the ability to hold more than half of the long-lived elements of the periodic table in its structure, and a structure that allows both cationic and anionic solid solutions and substitutions, apatite is also a versatile material for the field of environmental remediation [23]. Apatite permeable reactive barriers (PRBs) are now being used to remove dissolved uranium and ^{90}Sr. PRBs are a relatively simple, passive treatment technology for separating and immobilizing contaminants from groundwater [23].

Because of their high flexibility, apatites, $Ca_5(PO_4)_3F$ as shown in scheme 1.1 [25], may tolerate a wide range of cations (monovalent, bivalent, and trivalent) and anions in non-stoichiometric compositions. The nature and extent of substitution have a big influence on the physico-chemical properties of the derivatives [26].

Scheme 1.1

Chemical Structure Description for fluorapatite [25]

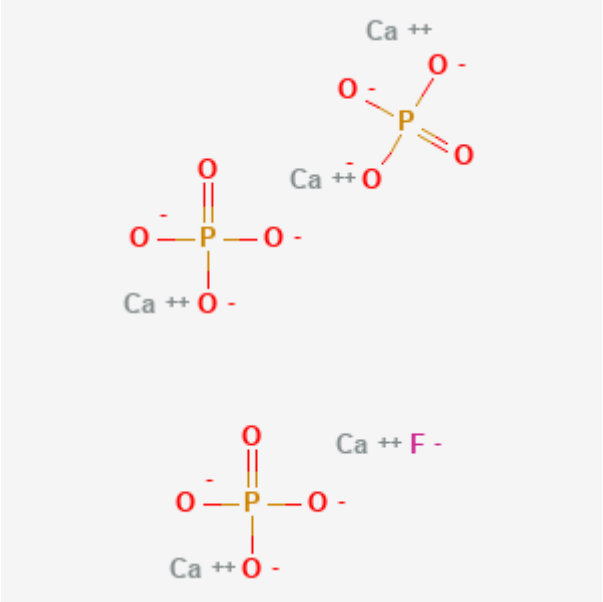

Fluorapatite crystallizes in a hexagonal crystal system. The unit cell parameters, crystal form (trigonal P3), lengths (a = 9.372, b = 9.372, and c = 6.883 Å), and angles (alpha = 90.000°, beta = 90.000°, and gamma = 120.000°). Fluorapatite, $Ca_5(PO_4)_3F$ (FAp), that is shown in scheme1.2 [27], is the least soluble apatite in acidic solutions, with a high thermal stability (melting point 1650°C), great chemical durability (solubility product in water, 3.16×10^{-60}), and good radiation damage tolerance [26].

Scheme 1.2

Crystal structure of fluorapatite: (A) side view (perpendicular to the fluorapatite (001) surface); (B) top view (parallel to the fluorapatite (001) surface) [27]

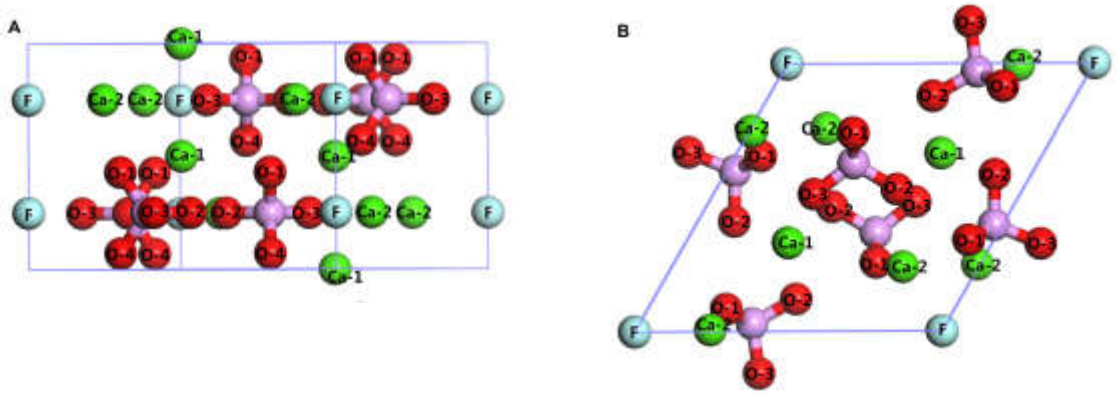

Apatite has a high potential as a radioactive waste form or as an engineered barrier in a nuclear waste repository since it can incorporate both anionic and cationic radionuclides. In apatite waste forms, apatite generated *in situ* by phosphate amendments, and phosphate-based cements, cationic radionuclides exchange for Ca^{2+}. The fact that apatite has remained stable in a variety of near-surface conditions for millions of years shows that it can sustain radionuclide irradiation by isolation from the environment for an extended period of time. Apatites also show self-annealing and chemical durability to the damage caused by α-decay events emitted from actinide radionuclides [23].

In the formula $A_{10}(BO_4)_6X_2$, where A stands for cations, BO_4 for an anionic group, and X for an anion (or ionic group such as OH^-), apatite refers to a family of compounds that most commonly crystallizes in the hexagonal space group P63 /m. The apatite with the greatest abundance in nature is known as fluorapatite, and its natural mineral form is a common accessory phosphate mineral that can be found in a variety of rocks. Appendix B Figure 1B shows the apatite structure in detail. There are two possible crystallographic locations for Ca (or the A cation), and each of these locations, sites I and II, are capable of accepting a variety of cations, including actinides, rare earth elements (REEs), Na^+, K^+, Cs^+, and Mg^{2+} [28]. Site I is preferred by REEs, however sites I and II can also be used with U and Th[4]. The B cation, meanwhile, typically forms a tetrahedron with four oxygen atoms. Different cations and anions can also substitute the B cation and X anion, respectively [28].

The structure is flexible and useful to confine radionuclides, notably the actinides (which are alpha emitters), under the area of nuclear waste immobilization due to the ability to include several radionuclides in the apatite form. It is important to modify the chemical composition of apatite in order to contain significant amounts of actinides. Site II's calcium cations (Ca) can be occupied by tetravalent or trivalent actinides (An^{3+} or An^{4+}), making the material a possible matrix for nuclear waste [29]. For instance, silicate apatite, $Ca_2La_8(SiO_4)_6O_2$, was suggested as a suitable phase to capture the actinides because the majority of nuclear waste glasses are silicate [30]. There are two ways to achieve the synthesis of fluoroapatite: by a solid solution reaction, or in an aqueous solution through precipitation or hydrolysis [4].The general procedure for immobilizing radioactive wastes in fluorapatite is depicted in scheme 1.3.

Scheme 1.3

General process for immobilizing radioactive wastes in fluoroapatite [4]

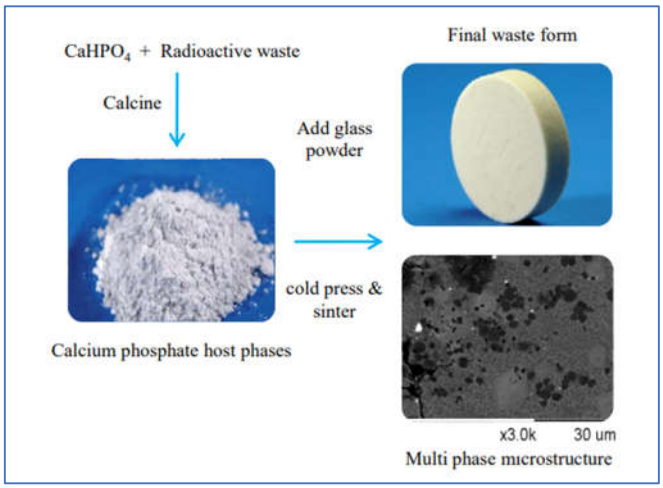

Apatites are used in thermochronology, a branch of geology that deals with predicting the thermal histories of rocks based on the temperature- and time-sensitive isotopic properties of minerals. While the apatite structure has long been thought to be a good alternative for confining nuclear wastes like actinides from spent nuclear fuel, this is not their only important application. Thorium and uranium were naturally decayed into heavy daughter nuclei and helium throughout the period of time by the alpha decay of the natural apatite minerals found in rocks. thermochronological helium (apparent) age can be computed and used to predict the time-temperature evolution (thermal history) of rocks across geological time using (U-Th-Sm)/He thermochronology, which measures the current concentrations of U, Th, Sm, and He in natural apatite crystals [31].

Because the apatite structure is suited for a wide range of substitutions, total or partial solid solutions can be formed. Table 1.1 contains a non-exhaustive list of the different

Table 1.1

Non-exhaustive list of possible substitutions for apatite crystals. Adapted from Miro, 2004.

Valence	A_{10}	$(BO_4)_6$	X_2
Monovalent	Na^+ , K^+ , Rb^+ and Cs^+		F^-, Cl^-, Br^-, I^- and OH^-
Divalent	Ca^{2+}, Mn^{2+}, Sr^{2+} , Ba^{2+}, Cd^{2+}, Pb^{2+}	CO_3^{2-} , SO_4^{2-} , HPO_4^{2-}	O^{2-} and CO_3^{2-}
Trivalent	REE^{3+} (La-Lu)	PO_4^{3-} , VO_4^{3-} , CrO_4^{3-} , MnO_4^{3-} and AsO_4^{3-}	
Tetravalent	Th^{4+}, U^{4+}, Zr^{4+}	SiO_4^{4-} and GeO_4^{4-}	

Although it depends on the actual composition, apatites are typically stable up to 1200ºC. Apatites have a very low water solubility when it comes to chemical stability, and this solubility decreases as temperature increases. Additionally, the damage caused by radiation can become unstable due to its structural design. Apatite crystal defects can be restored to its original position by just increasing the temperature a little bit.

By keeping phosphocalcium apatite at 130ºC for 10^4 years [32], an auto-regeneration phenomena that seems to be controlled by the Arrhenius Law can restore 50% of the defects. Crystal composition also affects auto-regeneration of defects and it is considerably increased with the presence of fluor in fluorapatites [33].

Since this structure is flexible, it is possible to embed several radionuclides in the apatite form. This structure and the stability connected with it led directly to the idea of using apatite to confine radionuclides, particularly the actinides (which are alpha emitters). It is important to modify the chemical composition of apatite in order to incorporate large quantities of actinides.

As the majority of nuclear waste glasses are silicate, silicate apatite (SiO_4^{4-}) was suggested as a suitable phase to trap the actinides [30]. Additional research has shown that significant amounts of plutonium and rare-earth elements (including La, Ce, Pr, Nd, Sm, Eu, and Gd) can be stored in apatite. Particularly for fluorapatite, several ceramics

were suggested for the deposition of some toxic fluoride salts produced during the electro-refining of Al-matrix nuclear fuels [30].

The behavior of apatite waste form under irradiation at a long-term scale is important and one way to study these effects is with natural analogues such as natural apatite. Thorium and uranium are naturally present in apatite minerals, and over time, these elements naturally decayed to form actinides and helium. The use of helium produced by alpha decay radiation as a low-temperature thermochronometer [34] has a long history and several direct applications.

It is still important to understand more about the kinetics of He diffusion and the potential effects of radiation-induced defects on the crystal.

1.3 Alpha decay

Alpha (α) decay is a nuclear process in which an unstable nucleus transforms into a different nucleus by ejecting a particle made up of two protons and two neutrons. This alpha particle is known as a helium (He) nucleus. Alpha particles are positively charged and have a significant mass. Because of their large mass, alpha particles cannot travel very far through the air or get very deeply into solids, nearly about 10 micrometers. Alpha decay is rarely employed in external medical radiation therapy since its path is limited to the near surface (micrometer range) as presented in scheme 1.4 [35].

Scheme 1.4

Different penetration levels of different products of decay, with gamma being one of the most highly penetrating and alpha being one of the least penetrating [35]

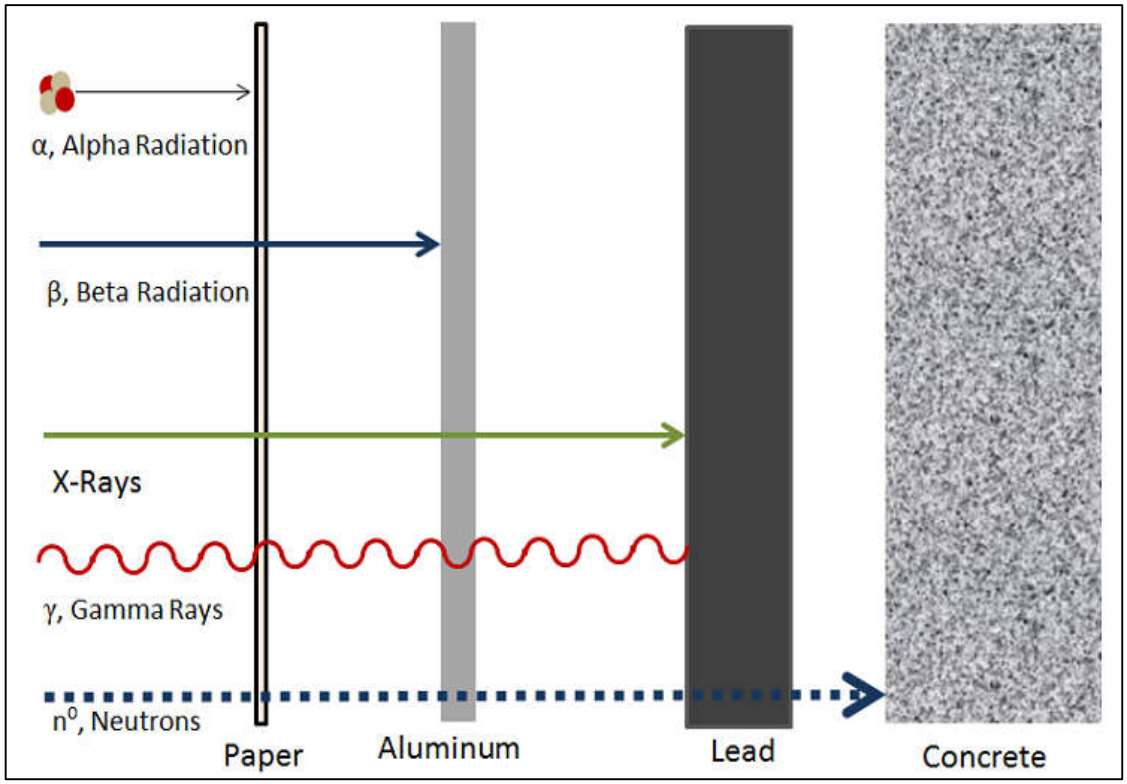

Ernest Rutherford originally distinguished alpha decay from other forms of radiation by observing the deflection of the radiation through a magnetic field. Alpha decay deflects in the way you would expect a positive particle to since alpha particles have +2e charge [35].

The general equation representing alpha decay is:

$$ {}^{A}_{Z}X \rightarrow {}^{A-4}_{Z-2}Y + {}^{4}_{2}He \quad \text{.....1.1} $$

Where: ${}^{A}_{Z}X$ is the parent nucleus, the starting nucleus. A is the total number of nucleons (the number of neutrons plus the number of protons). Z is the total number of protons. ${}^{A-4}_{Z-2}Y$ is the daughter nucleus, the ending nucleus and ${}^{4}_{2}He$ is the released alpha particle. After alpha decay the typical energy gained by the heavy recoil nucleus is about 100 keV and the one of the alpha particles is ranging from 4 to 9 MeV.

Americium is a common element in the commercial market because it is a primary producer of alpha particles. Alpha particles are released inside the smoke detector, a common application of alpha decay. As a result, the air inside the detector becomes

ionized. Because smoke in the detector absorbs this alpha radiation, the ionization is altered and the alarm is triggered if smoke is present [35].

Alpha particles are also utilized in a technique called Alpha Particle X-Ray Spectroscopy (APXS). The elemental composition of rocks and soil is determined using this method. NASA used this method in its missions to Mars, including the Pathfinder missions, to determine what elements existed Martian rocks [35].

In the medical field, alpha particles are also useful. Targeted alpha therapy (TAT) is a new cancer treatment that uses alpha decay to kill cancer cells. When ^{212}Pb is ingested, it travels to the tumor location and emits alpha radiation, which kills all the cells in the area [35].

The process of annealing was applied to repair the radiation damage Experimental evidence suggests that apatite may anneal during alpha particle bombardment (termed "self-annealing"), which, combined with a low solubility in aqueous fluids and propensity to incorporate actinide elements, makes this mineral a promising phase for nuclear waste storage.

1.4 Radiation-induced deffects

The effects of α-decay on the lattice are a significant factor in the formation of defects within the crystalline structure of waste materials. When an energetic α-particle collides inelastically with lattice ions, it is initially slowed through electronic stopping. Localized heating and electronic defects are produced during this initial phase. Nuclear stopping predominates as particles lose energy through these interactions to the point that their kinetic energy falls below 100 keV. At this point, the incident particle and the lattice can collide in elastic ways. These can give lattice ions, also known as primary knock-on atoms (PKAs), a large amount of kinetic energy, causing a series of collisions that are likely to produce point defects. Beta and alpha decay affect the crystalline materials by transferring energy to atomic nuclei and electrons (ionization and electronic excitations), primarily via ballistic processes involving elastic collisions [36]. Ionization processes dominates the energy transfer of beta particles while for ions such as alpha particles and recoil nuclei, interactions involve both ionization processes and elastic collisions. Depending on how much energy is transferred during the collision, defects may be created or not. If the energy transferred to a lattice atom is higher than the minimum energy required to permanently displace an atom from its regular lattice site (displacement threshold energy,

Ed), the atom will be ejected from its position in the lattice. This will lead to the formation of an empty lattice site called a vacancy. The displaced atom can potentially displace lattice atoms and so on, leading to the creation of a so-called collision cascade.

A Frenkel pair defect is a point defect that includes both the interstitial-type atom and a vacancy. As long as the interstitial point defect is sufficiently separated from the vacancy to allow interstitial-vacancy recombination, a Frenkel pair can be formed. The displaced atom (called the primary knock-on atom or PKA), might have enough kinetic energy to cause a secondary displacement. Another displacement may be produced by the secondary displaced atom itself. This process continues, and a single projectile may then induce a series of displacements before coming to rest. As an ion moves through the material, a highly disordered region develops around its path. This collision cascade happens near the end of ion's trajectory by uniquely elastic collisions and the set of point defects created is known as a displacement cascade. Interstitials and vacancies can form during collision cascades, so close one to each other that it might easily recombine.

Many of the interstitials and vacancies created during collision cascades damage as a result of the clustering of point defects' close proximity. Only a small percentage of the initially formed point defects are capable of surviving and successfully produce a radiation-induced defect. Even though the number of surviving Frenkel pair defects is low, it is still high enough for it to accumulate and lead to a transformation of the structure. While vacancy defects can concentrate in a large area to form cavity defects, interstitial defects can gather to form defect clusters. Interstitial defects can lead the formation of dislocation loops and dislocation networks when their concentration continues to increase upon irradiation. The swelling, polygonalization, local amorphization, and modification of the chemical, electronic, thermal, mechanical, and other properties of a material can all occur from this damage and transformation of the structure [36].

1.5 Rutherford Backscattering Spectrometry (RBS) characterization

Rutherford Backscattering Spectrometry (RBS) is a popular nuclear method for analyzing solids' near-surface layers. The energy of backscattered projectiles is recorded with an energy-sensitive detector, typically a solid-state detector, when a target is bombarded with ions with an energy in the MeV range (typically light ions H; He in the range 0.5–5 MeV) [37].

RBS provides a quantitative analysis of a material's composition as well as the depth profiling of individual elements. RBS is nondestructive, has a strong depth resolution of the order of several nm, and a very good sensitivity for heavy elements of the order of parts-per-million, and is quantitative without the need for reference samples (ppm) due to the use of the well- known Rutherford cross section. The analytical power of the method is based on the knowledge of the Rutherford cross section that fits very well experimental data in the MeV energy range [38].

For incident He-ions, the analyzed depth is normally a few μm, while for incident protons, it reaches typically tens of μm. The limited sensitivity of RBS for light elements is a drawback, which requires the use of additional nuclear-based methods such as nuclear reaction analysis (NRA) nuclear elastic resonances (such as $^{4}He(^{16}O, ^{16}O)^{4}He$), elastic recoil detection analysis (ERDA) or PIXE (Particle Induced X-ray Emission) [37].

Rubin et al. [39] described RBS as a method for materials analysis for the first time in 1957. All forms of elastic ion scattering with incident ion energies ranging from 500 keV to several MeV are included in RBS. Protons, ^{4}He, and sometimes heavier ions (lithium) but also deuterons (usually used tin parallel to NRA) are utilized as projectiles, with typical backscattering angles ranging from 150 to 170 degrees. In rare circumstances, alternative angles or projectiles are used.

1.6 Ion channeling characterization

Ion channeling is a specific feature of ion-solid that only occurs in single crystals. When energetic ions are aligned along a major crystallographic axis (or plane) of a single crystal, ion are steered into the crystalline structure by atom nuclei of the solid and travel along the crystal structure with low-angle deflection since atomic positions are correlated. While coupled with RBS, the yield of backscattering events is strongly reduced (typically by one to two orders of magnitude) when a defect-free single crystal is analyzed. Hence, assuming a defective single crystal (native defects or defects generated by ion implantation for instance), channeling coupled to RBS is a key method to measure the amount of defect into the surface layer of crystals (typically up to micrometer range) by recording both the so-called aligned spectrum (recorded with ion beam aligned with the crystal main orientation) and random spectrum (measured several degrees off the main axis to avoid any significant channeling effect).

Ion channeling is the technique by which charged particles are steered over long distance within a crystal without being backscattered. Three basic components are required for a channeling experiment: a source of energetic ions that are well collimated, a detector for backscattered particles, and a crystal manipulator, also known as a goniometer, that can rotate the crystal in different directions to facilitate axis alignment with the beam.

The ion beam sees the lattice as frozen during channeling because the rms (root-mean-square) displacement of the atoms is much lower than the particle velocity. It happens when a main crystallographic orientation is coincident with the ion velocity vector. The ions will move in that direction once they are inside the channel, experiencing several collisions that are nearly elastic as well as electronic interactions with the valence shell electrons, until they come to rest or finally dechanneled by matrix atoms or defects. Dechanneling may be caused by a defect or impurity in the crystal, or by thermal vibrations of matrix atom. When the crystal is not aligned (random), the energy and the yield of the backscattered particles is similar to a spectrum that would have been recorded on a polycrystalline solid or on an amorphous solid of the same composition.

When the crystal is aligned, a huge reduction in the number of backscattered particles could be observed because atom strings "shading" one another. Any atoms off their lattice sites, however, will give visible extra scattering. Therefore, crystal damage is visible, and point defects (interstitials) can even be distinguished from dislocations provided investigations are performed at several different beam energy of probing ions. The surface peak, the direct scattering peak, and the dechanneling signal are the three fundamental contributions to a channeling spectrum. Scheme 1.5 shows an illustration of the dechanneling caused by defects and the spectra that will be obtained.

Scheme 1.5

Various types of defects and their influence in the shape of dechanneling spectra in a schematic way [40]

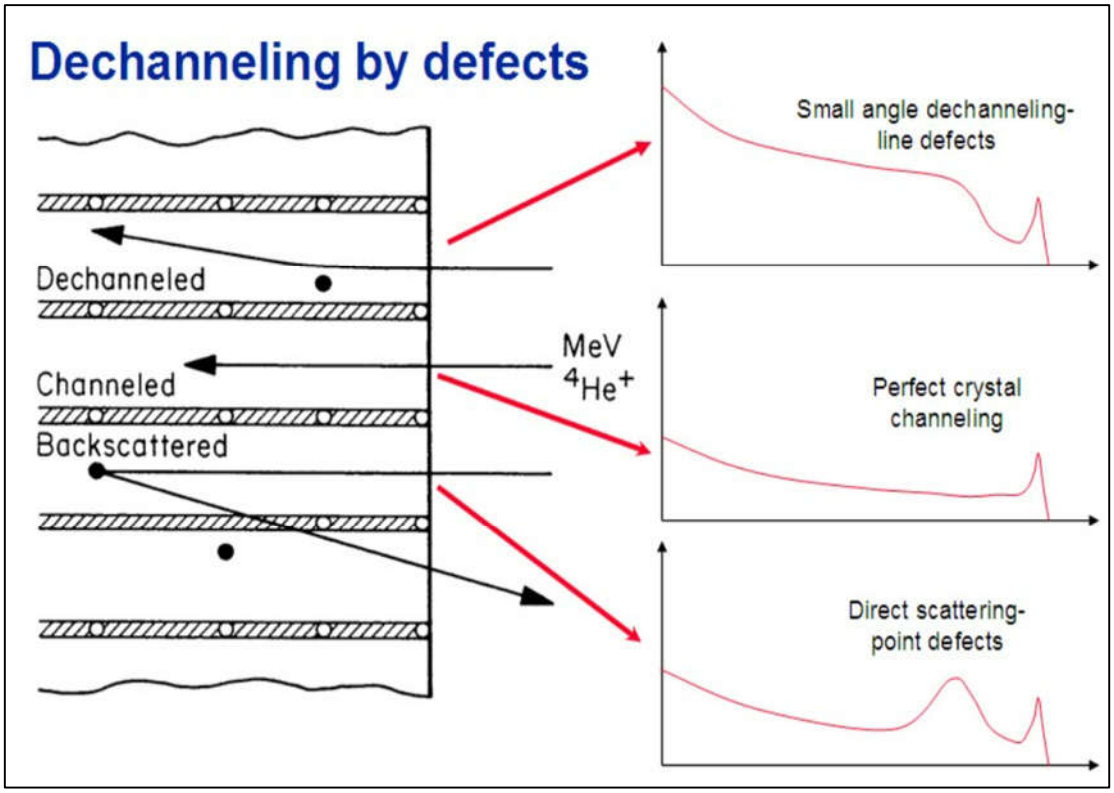

1.7 Simulation software

1.7.1 RUMP

RUMP (Rutherford Universal Manipulation Program) is a tool for RBS plotting, analysis, and simulation [41]. It enables the user to plot the real RBS random and aligned spectra as well as the user-provided simulation spectra depending on several factors like energy calibration, composition, and experimental parameters. These experimental data include the detector's geometry and the energy of the incident ions. This simulation spectrum depends on the user entry chemical composition as each chemical element provides a different contribution to the yield. Finding the composition that would match the actual spectrum or the chemical composition of the crystal is one of the features of this method [42-45].

1.7.2 Monte-Carlo (McChasy) code

The McChasy simulation code, that is developed at the NCBJ Warsaw, is a Monte Carlo code that is used to directly simulate the trajectories of ions into a crystal and thus to calculate the expected ion channeling spectra assuming a given (defective) structure. Table 1.2 shows McChasy user interface and an example of calculation in progress. It can be utilized to determine a material's disorder profile. McChasy means «Monte Carlo Channeling Simulation code». The backscattering energy spectra obtained at channeling, random, or any specific angle between the projectile and the normal to the target's surface can be calculated.

The code assumes a given crystal structure and allows several types of structural defects to be incorporated: amorphization of a fraction of matrix atoms of a given sublattice (referred to as randomly displaced atoms), dislocations characterized by their size and density. Structural defects concentrations can be defined at any depth. The comparison of the calculated spectra with the experimental ones allows one to extract relevant information on the distribution of defects in the real crystal. In a first step, it is necessary to define several parameters, including the following ones: crystal parameters (crystallographic structure, composition), experiment geometry input and output angles), incident beam characteristics (nature, energy, ion beam divergency), and detector parameters (resolution).

A crystal is divided into several slices at increasing depth when using the code through the Monte Carlo method. The initial impact parameter (p_0) is chosen at random assuming a uniform distribution, and the changes to it are then calculated. The code models the ion-atom interaction using a Coulomb screened potential to calculate the trajectory of the incoming particle along its path. McChasy always takes the same crystal cell into account; the only difference is the initial tossing of impact parameter.

The main benefit of the Monte Carlo simulation is that, in contrast to a traditional dechanneling studies that are performed using various types of simplified model of defects and analytical decomposition of experimental spectra, it enables a quantitative analysis of crystals containing a variety of different types of more realistic defects [46].

Table 1.2

McChasy user interface and an example of calculation in progress

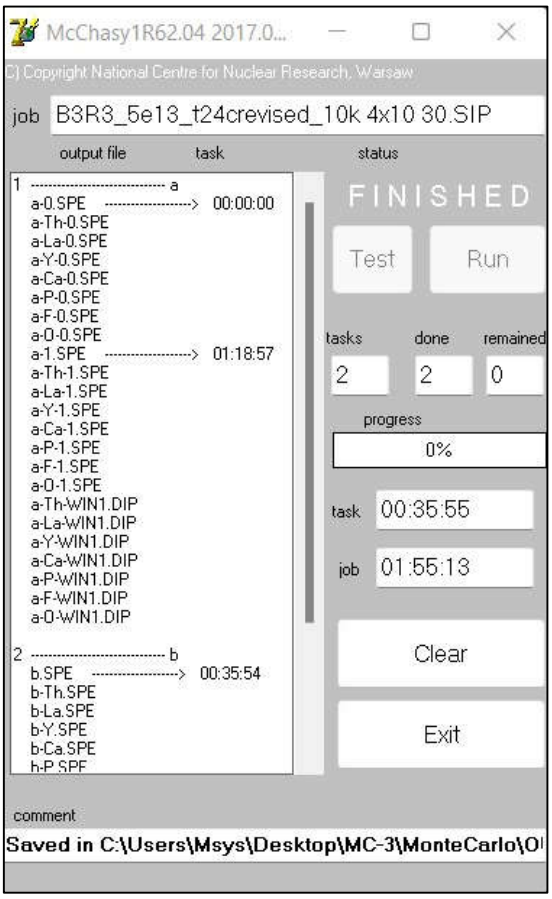

1.8 Bismuth element as heavy recoil nucleus

Bismuth (Bi – atomic number Z=83) is a brittle metal with a somewhat pinkish, silvery metallic shine. Bismuth is the most diamagnetic of all metals (i.e., it exhibits the greatest opposition to being magnetized). It is hard and thickly crystalline. It undergoes a 3.3 percent expansion when it solidifies from the molten state. Although bismuth-209 is now known to be unstable, it has classically been considered to be a stable isotope because it has a half-life of approximately 2.01×10^{19} years, which is more than a billion times the age of the universe.

In our studies the bismuth ion was selected to experimentally simulate the heavy recoil nucleus emitted after an alpha decay. Although alpha decay of U or Th would imply the formation of Th or Ra, respectively, bismuth was chosen as the heaviest (almost) stable element that can be easily prepared on the source of an ion implanter with no significant

change in irradiation parameters. (Atomic mass and atomic number similar to Ra and Th, responsible for the creation of the same collision cascades when their slow-down).

1.9 Objectives of the study

The main objectives of this study are:

1. To experimentally investigate the radiation effects induced by the decay of actinides in fluoroapatite crystals $Ca_5(PO_4)_3F$ using ion implantation
2. To propose a model of creation of crystalline defects in natural apatite and its healing rates based on the chemistry of the samples and the temperature.
3. To determine whether apatite can be used as an alternative matrix for embedding those HLW (fission products and minor actinides) that are currently stored into nuclear glasses.

Chapter Two
Experimental work: Materials and methods

Natural fluorapatite used in the experiments are originating from the Durango mine in Mexico. They have macroscopic dimensions of a few centimeters, and they form a single crystal. Sample preparation, materials characterization by RBS and channeling, Bi implantation to apatite crystal, RBS data treatment using RUMP software, and McChasy software simulation to characterize defects evolution in the samples were the key tasks completed during this work.

At the chemistry laboratory located at the Energy & Environment division at IJClab, several experiments were performed on different crystals and for different ion implantation conditions. Before that step, the sample preparation was done by four main steps (as will be explained later) to make the crystals ready for characterization by RBS/C. The crystals were prepared and ready for characterization. Irradiation experiments were achieved at various temperature.

2.1 Sample preparation

The natural single crystals of fluorapatite were prepared and submitted to several processes to make sure that they will be suitable for the subsequent procedure of RBS characterization, i.e., to attest that their crystallinity is satisfactory. Below are the most important steps that were followed to prepare the sample.

2.1.1 Crystal cutting

Crystal cutting was the first step to prepare the sample. In this step, there were two large single crystals studied and both came from Mexico Durango location. Both crystals show very nice natural faces (Appendix B Figure 2B) that allows one an easy determination of the symmetry elements. In particular, the hexagonal (001) plane perpendicular to the *c* axis can be ascribed. At first, a hot plate was set at temperature 130^{o}C. When the hot plate reaches the set-up temperature the crystal sample was fixed on a piece of ceramic from a flat side by glue. Then, the sample was taken and put it on the machine. The machine was used in this step is a diamond edge saw machine as demonstrated in Appendix C Figure 1C. The principle of it is the single crystal was placed on the designated sample holder while the diamond wire was placed perpendicular to the [001] direction of the crystal. A

rotation machine is responsible in moving the wire which cut the crystal into slices. Then, the machine was opened, and the first crystal and the second crystal were cut into two-mm slices with a diamond edge saw. In total, there were eight slices prepared from single crystals during this internship work. Both crystals were cut perpendicularly to the [001] direction using the natural faces of the crystals as guides. After cutting, the crystals were put again on the hot plate to remove the slices from the ceramic then these samples were taken and placed in acetone and then in ethanol to remove all glue residue from the samples. Finally, the crystals were dried by towel and put each slice in small box.

2.1.2 Mechanical Polishing

The as-cut crystal slices were then fastened with the use of a heat sensitive glue on a piece of metal to prepared sample holders as required for the mechanical polishing step. The surface of crystals needs to be cleaned and polished to remove the roughness and give reliable RBS spectra (the penetration depth of probing ions must be the same irrespective of their position at the surface of the sample). A disk polisher (ESC 300 GTL) was used Appendix C Figure 2C. It is composed of a mechanical rotating machine and a metal disk overlaid with a cloth paper. Polishing was achieved through mechanical friction between the crystal surface, the cloth paper, and the polishing solution containing diamond microparticles sprayed at the surface of the cloth paper. Mechanical polishing was done in four stages: First stage using 15 µm diamond particles, second stage using 6 µm, third stage using 3 µm, and fourth stage using 1 µm. After each stage, surface condition was checked for the presence (or absence) of defects using an optical microscope, Olympus BX-51, and then cleaned with the use of an ultrasonic bath with ethanol. Eight well-polished samples were obtained. Figure 2.1 showed an example of a microscope capture of crystal surface before and after polishing.

Figure 2.1

Microscope images of apatite surface in as-cut state and in the four polishing stages. As-cut: rough surface and presence of many irregularities. Final stage 1 μm: Flat surface and presence of only few natural defects and fractures

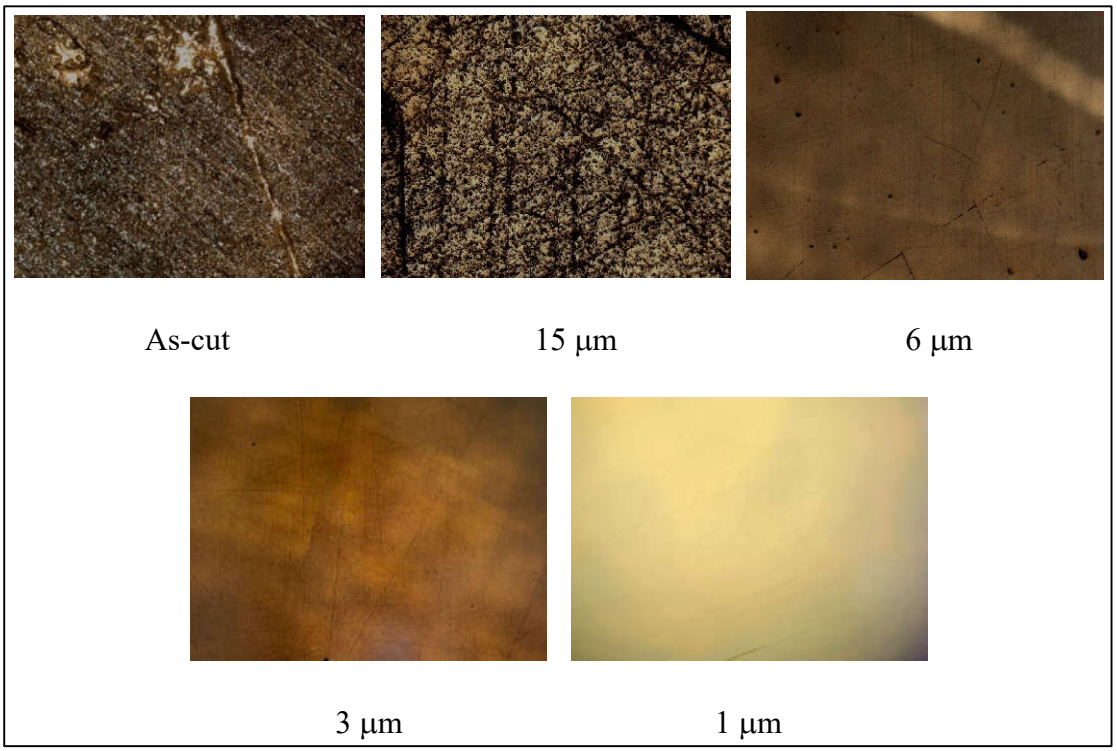

2.1.3 Thermal annealing

After polishing, crystal slices were thermally annealed for 24 hours under air using a furnace as presented in Appendix C Figure 3C, at a temperature of 900ºC. Temperature was increased at a rate of 2°C per minute up to the plateau. Similarly, after the plateau at 900°C, temperature was slowly decreased at a rate of 2° per minute (in practice below about 400°C the temperature decrease is slower due to the large volume of the furnace). The goal of this step is to remove all the damage caused by the previous step mechanical polishing stage. Samples were put inside a boat made from alumina and then put it in the furnace and withdrawn when the programmed time expired. The color of the crystals changed from yellow to transparent (as shown in Scheme 2.1): such as change was expected because color centers in the crystals (defects which give the yellowish tone color) are removed by the heating treatment of crystals. A color center is a type of defect a vacancy in the crystals is filled by one or more unpaired electrons. These electrons

absorb light in the visible spectrum because of this the crystals will be colored when its normally transparent. Color centers are typically formed by irradiation: in the present case apatite crystals contain a very small fraction of Th and U atoms that are responsible for natural radioactivity and therefore damage creation. Aluminum oxide is the material for boat and for the tube inside the furnace: this ceramic is selected for its thermal stability at high temperature and their inertness with respect to apatite crystals.

Scheme 2.1

Crystals thermally annealed for 24 hours under air using a furnace at a temperature of 900°C, before and after thermal treatment. As they appear the crystals have a yellowish tone color before and they have an transparent color after annealing

Before annealing After annealing

2.1.4 Carbon layer (graphite layer) deposition

The final step in sample preparation is the graphite layer deposition to the polished face of the annealed crystal samples. Approximately 10 nm were put at the surface of the crystals to avoid surface charge accumulation during the next step of materials characterization by RBS. He ions during RBS experiments would accumulate at the surface of the crystal because of fluorapatite is an insulator, leading to a distorted RBS spectrum that would have been impossible to analyze. A very thin layer of graphite was put on the crystals by using a carbon coater machine (Cressington carbon coater) that is depicted in Appendix C Figure 4C. This machine was coupled to a pump responsible for the provision of vacuum inside the system. Electric current was then passed through a

thin graphite wire resulting to its evaporation and deposition to the samples located below it. With the carbon conductivity, no electric charge accumulates at the crystal surface and He ions can then penetrate inside the crystal and be backscattered to the detector providing reliable elastic backscattering spectra.

After sample preparation the crystal quality was tested by ion channeling using a goniometer which is a device used to precisely fix the angle between the crystal surface and ion beam direction. Goniometer measures an angle or permits the rotation of an object to a definite position. In orthopedics, the former description applies more. The art and science of measuring the joint ranges in each plane of the joint are called goniometry. Goniometer which can rotate the crystal in different directions to facilitate axis alignment with the beam. In the present case, two independent translations and two independent angular rotations are available on the goniometer system of the platform.

2.2 The JANNuS-Orsay irradiation platform

2.2.1 Rutherford Backscattering Spectrometry (RBS) experiments

At the JANNuS (Joint Accelerators for Nanoscience and Nuclear Simulation) facility managed by the IJCLab platform at Orsay, several RBS experiments at room temperature were conducted. The JANNuS installation makes it possible to develop real-time studies on the effect of implantation and / or irradiation of ions in different materials, particularly in relation to nuclear energy. In Appendix B figure 3B is shown the parts of the instrument that were used in our experiment.

During ion implantation and irradiation, both the ion implanter (IRMA) and accelerator ARAMIS ion beams are rastered for ensuring a full and uniform implantation fluence at the sample's surface up to 100 x100 mm^2. The accelerators of IRMA and ARAMIS are connected by five beam lines (see Appendix B Figure 3B). Two beam lines are devoted to ion implantation/irradiation, and one beam line is used for IBA, which allows for the structural and chemical characterization of materials using Rutherford backscattering spectrometry (RBS, RBS/C), elastic recoil detection analysis (ERDA), and particle-induced X-ray emission (PIXE). The two additional lines are employed for the TEM (Transmission Electron Microscope) and IRMA and ARAMIS accelerator coupling, respectively (see Figure 2.2) [47, 48].

The IRMA ion implanter (190 kV) of JANNuS-Orsay was used in the research project to simulate ballistic damage in apatite induced by alpha recoil nuclei. Different fluences of 500 keV Bi ions at various irradiation temperatures were applied for apatite crystals implantation. This was done to get an efficient simulation of the growing crystal damage which is a result of alpha recoil nuclei and to achieve the kinetics of radiation damage. The amount of the produced damage by utilizing different damage fluences of the implanted crystals were then characterized by RBS/C (in ex situ mode). The 1.4 MeV He^+ ion beam from JANNuS-Orsay's ARAMIS accelerator (2 MV Tandem type) which acts as characteriztion beam was used in the RBS/C experiments. The obtained RBS/C spectra from the characterization experiments were then simulated using McChasy, a Monte Carlo code, to measure quantitatively the amount of defects as a function of depth for each of the damage fluence used in the experiments.

The ionization-induced recovery of pre-existing defects attributed to the electronic energy deposition of alpha particles in apatite was also experimentally simulated using the same 1.4 MeV He beam of ARAMIS which was used to irradiate one set of apatite crystals - one pre-damaged with alpha recoil nuclei irradiation (500 keV Bi ions). It is to be emphasized that this same ion beam, aside from depositing electronic energy along its path (which could then induce defects recovery of pre-existing defects), also simultaneously served as the characterizing beam of the ex-situ RBS/C set-up in determining the extent of damage recovery as a function of the He beam charge. All the collected RBS/C spectra recorded during the characterizations steps were also simulated using McChasy to derive the damage recovery kinetics at various depths of the irradiated crystal.

In the first phase of experiments, before irradiation, a beam of 1.4 MeV He^+ was used to characterize eight crystal slices produced in the sample preparation stage (one of these crystals divided to two pieces) and determine its suitability for the ion channeling technique. 1.4 MeV was chosen as the incident energy for RBS experiments to meet the criteria that the incoming ion energy is low enough that pure Rutherford elastic scattering occurs outside the nucleus (no nuclear reaction), but high enough to avoid significant effects of screening of nuclei by electrons, which, at low distance of approach, reduce the effective charge of the nucleus. The second phase, on the other hand, involved an ex-situ experiment of ion implantation using 500 keV Bi followed by RBS/C characterization

(IBA) beam line of the platform using 1.4 MeV He^+ in channeling conditions on a pre-irradiated fluorapatite crystal. The purpose of this second phase is to investigate the effect of implanted Bi ion (to simulate a recoil nuclei) by RBS technique to natural fluorapatite as a function of implantation (irradiation) fluence.

Figure 2.2

The ex-situ mode of RBS/C experiments involves two major steps: (1) implantation of Bi ions at different fluence to several apatite samples using an ion implanter and (2) RBS/C characterization of each of the implanted samples using the characterization (IBA) beam line of the platform

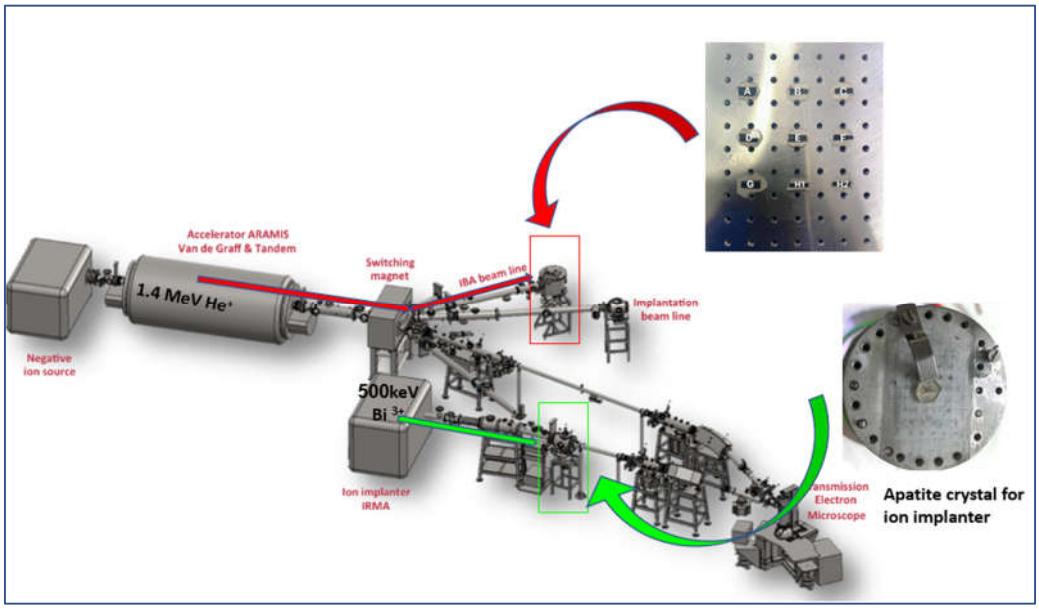

2.2.2 First phase RBS/C: measurement of the crystalline quality of the as-prepared crystals.

After sample preparation, the crystal slices were fixed on the aluminum holder by using a conductive carbon scotch tape to fix the crystals on the holder, then label the crystals to mount them on the goniometer under vacuum at about 10^{-6} mbar. This step is made to quantify the quality of these crystal slices.

The characterization beam here is He^+ 1.4 MeV as kinetic energy. Such an energy was selected since it allows a good separation of the various chemical elements of the apatite crystal, while keeping a good depth resolution that allows the depth distribution of defects to be extracted by channeling with a good precision. The samples A B C D E F G H1 H2, which presented in Appendix B Figure 4B were labelled. Double-face scotch (carbon scotch) was used, it is a conductive carbon layer. The use of the carbon scotch at the

backside of crystals was favored over the use of metallic pins for the following reasons: First; a pin creates some shadow at the surface of the sample; second: in some cases when the sample is small it could be problematic since it leaves space to a small irradiated zone only; Third, it creates some pressure on the sample when it is fixed tightly and may cause breakage of the crystal especially for single crystal due to the mechanical pressure. In other cases, it might be loose, and samples may fall down in the analysis chamber.

An alignment procedure of the goniometer was made to align the ion beam direction with the main [001] axis (the *c* axis) for each of the respective fluorapatite samples. Displacements in the *x* and *y* direction were made to be sure that the beam is impinging on a crystal slice with no part of the beam on the holder. This is verified by obtaining RBS yield spectra in the "random mode" in which the goniometer is rotated continuously (4^o cone) with respect to the major crystal axis. If the spectrum presents a characteristic front for the various atoms that constitutes apatite (typically at the energy corresponding to the Ca front that appears at medium energy) and did not present the aluminum signal (invisible) of the holder, then the beam is said to be impinging on the sample (it can be checked by recording spectra at various positions from one extremity of the crystal to the next one). Following this, the major *c* axis for ion channeling was sought by performing angular displacements (0.2° increments) in rotation angles α (around the y-axis) and rotation angles β (around x-axis) of the goniometer to determine (α, β) coordinates with minimum backscattering yields for each of the following four regions of (α, β) coordinates:

(-3, -3) to (-3, 3), (-3, 3) to (3, 3), (3, 3) to (3, -3), and (3, -3) to (-3, -3). The recorded minima (circles in Scheme 2.2a) correspond to intersection of the ion beam direction with the main crystallographic planes of the apatite structure. To facilitate a graphical method of finding a channeling axis easier, the (α, β) coordinates were plotted on a square that showed the lowest backscattering yields (channeling dips corresponding to the alignment of the energetic ion beam with a major crystallographic plane of the crystal). Then the overlapping of the square containing channeling dips with the standard stereographic map for a closed-packed hexagonal crystal allows the identification of the expected angular positions of the closest channeling axis (here the <001> or *c* axis). Shallow channeling dips, corresponding to crystallographic planes (with a typical yield of 0.8 with respect to the random yield), were connected by trace lines and the intersection of trace lines

(corresponding to crystal planes) corresponds to the angular position of the main crystal axis (Scheme 2.2). After this step, the sample could be suitable for further ion implantation when the integral of the RBS yield measure of spectrum just below the surface peak (the so-called minimum axial yield χ_{min}) is low enough, typically around 10% for the specific case of fluorapatite crystals, as it was established from the previous investigations performed within our research team. Monte Carlo simulations will confirm the good quality of measured crystals.

Scheme 2.2

(a) Angular positions of minima of channeling dips recorded by measuring the backscattering yield along the edges of a square. (b) the standard stereographic map for a hexagonal crystal with specific positions of atoms for apatite. (c) Overlapping of the square containing channeling dips with the standard stereographic map for a hexagonal crystal with specific positions of atoms for apatite allows the identification of the expected angular position of the main channeling axis

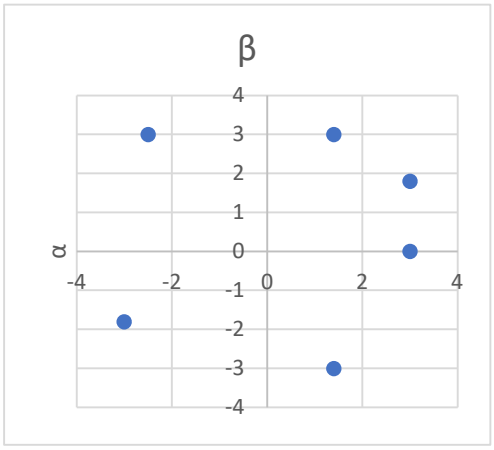

(a)

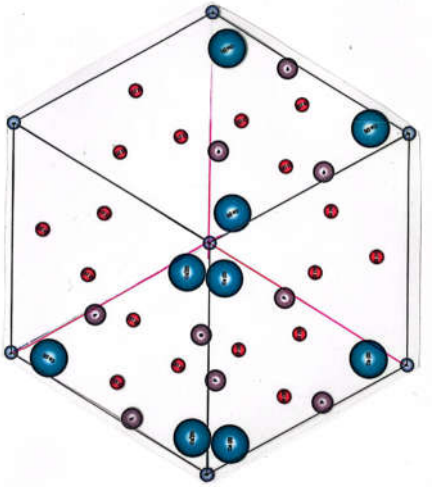

(b)

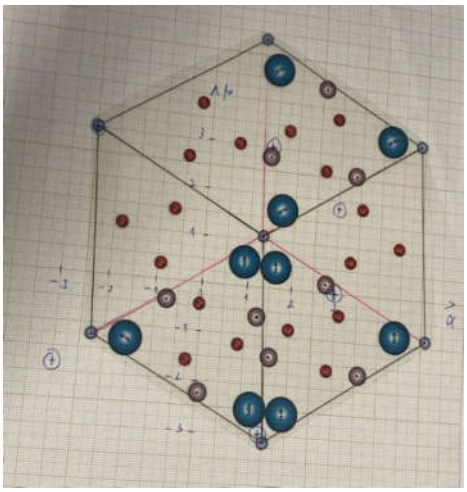

(c)

Figure 3.1 in Chapter Three represent typical random and aligned RBS spectra that show the various fronts corresponding to the various chemical elements. The blue line is the random spectra and the gray the aligned one.

2.2.3 Second phase: ion implantation and RBS/C

In this step selected samples (only the ones with a good crystallographic quality as measured in the previous section) were implanted with 500 keV Bi^{3+} ions at room temperature one by one at different fluences, as shown in Table 2.1, to measure the damage that will be formed from this irradiation condition. These experiments were done by implanting the fluorapatite crystals with low-energy Bi^{3+} ions to simulate the heavy recoil nucleus emitted during an alpha decay of an actinide. A1.4 MeV He^{+} ion beam was used at room temperature to both to collect RBS/C spectra in channelling geometry to measure the lattice disorder induced by Bi irradiation but also to simulate and track a possible effect of the slowing-down of the alpha particle on the disorder recovery induced by electronic stopping.

The first set of apatite is composed of 500 keV Bi^{3+}-implanted crystals to represent crystals with various initial damage states caused by a prior alpha recoil nuclei irradiation at various fluences. The samples were implanted stepwise with Bi^{3+} to achieve each of all the following fluences:

Table 2.1

Implantation fluences that were used to implant the crystals with 500 keV Bi^{3+} ions at room temperature

Fluence Number	Fluence (cm^{-2})	Sample
1	3×10^{12}	A
2	1×10^{13}	B
3	4×10^{13}	C
4	5×10^{13}	D
5	8×10^{13}	E
6	1×10^{14}	F
7	1.5×10^{14}	G

In order to prevent implanted Bi^{3+} ions from channeling into fluorapatite, the implantation conditions include a tilt angle of around 7° with respect to the main axis: such a condition simulates the slowing-down of the heavy recoil nucleus after an alpha decay in a direction not aligned with a main crystallographic axis (almost all cases).Before proceeding on to the next implantation fluence with Bi ions to explore the high fluence behavior of irradiated crystals, RBS/C characterization at channeling conditions for each of the given fluences was conducted in order to determine the effect of implantation on the backscattering yield at aligned and random positions.

The same procedure was performed for crystals implanted at 100ºC: the apatite slices were implanted with 500 keV Bi^{3+} ions at different fluences as noted in table 2.2. After implanting the fluorapatite crystals with low-energy Bi^{3+} ions and using 1.4 MeV He^{+} ions irradiation at room temperature, the RBS/C spectra were collected in channelling geometry.

Table 2.2

Implantation fluences that were used to implant the crystals with 500 keV Bi^{3+} ions at 100ºC

Fluence Number	Fluence (cm^{-2})	Sample
1	3×10^{12}	B
2	6×10^{12}	D
3	1×10^{13}	F
4	3×10^{13}	E
5	4×10^{13}	A

2.3 Alpha recoil damage accumulation at room temperature

By implanting 500 keV Bi^{3+} ions at different ion fluences ranging from 10^{12} to 10^{14} cm^{-2} into a set of apatite crystals, the damage accumulation caused by alpha recoil nuclei in apatite was experimentally simulated. Ex situ RBS/C was used to characterize the damage that each ion fluence had caused to the crystals. RBS/C experimental spectra of an apatite irradiated at room temperature with 500 keV Bi^{3+} ions at various ion fluences were recorded (see Figure 3.5 in Chapter Three).

After the experimental data were obtained from RBS/C, Monte-Carlo simulation McChasy code was used to simulate the experimental data with the goal to quantitatively measure the kinetics of the disorder induced in the crystal by the implantation process.

The McChasy code was used to treat the collected spectra. This code was made especially adapted for this work on apatite crystals to define the hexagonal crystal structure, space group, and position of the various atoms in the cell. All experimental data (e.g., ion beam characteristics, target characteristics, geometry of experiment) were entered inside this code as in the input file (see Table 2.3). For each Bi fluence, corresponding to a different RBS/C spectrum, the fraction of radiation-induced defects at a given depth, RDA, was set as input in the MC simulation to generate computer-based channeling spectra that can be ultimately compared with experimental recorded spectra. This step requires many different runs, modifying step by step the depth distribution of defects, to finally achieve a satisfactory fit to the experimental spectrum: a lot of time was spent on this mandatory step that requires skills and self-critical analysis. After this step the evolution of the damage-depth distribution with ion fluence was then subsequently obtained and analyzed. A typical input file shown in Table 2.3 is an example of the data that was put inside the file to gain the best depth distribution of defect, RDA, that mimics of the experimentally recorded aligned spectra.

Table 2.3

Example of an input file from McChasy code for different RDA that were used. The first column at left is a command to the code corresponding to a parameter to be fixed followed by its name or by its value (in this example PRO helium is the He probing ion and ENE 1394 its energy in keV)

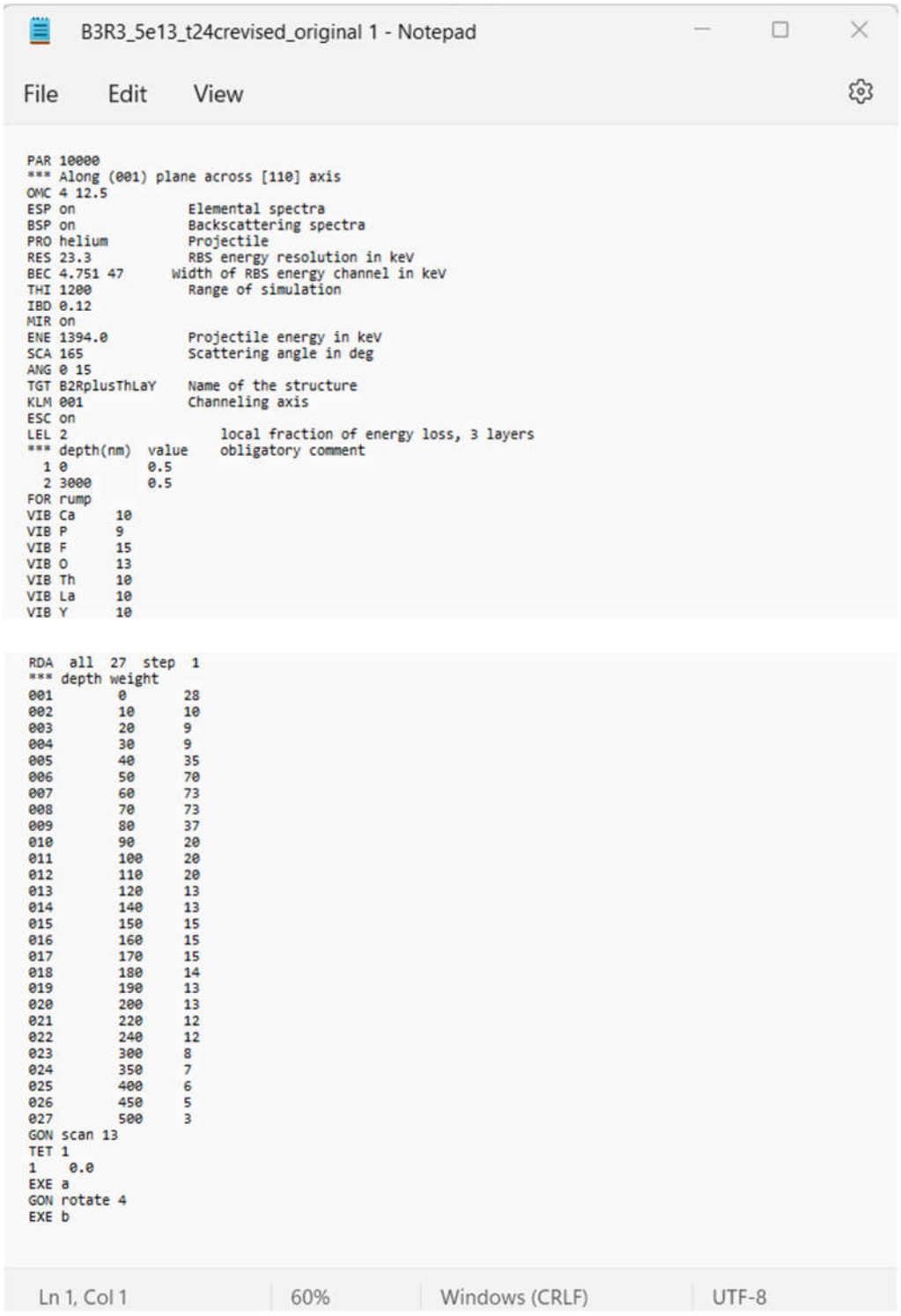

2.4 Idealized ion channeling model for fluoroapatite

A quantitative description of the crystal evolution requires the use of a Monte Carlo simulation code: virtual particles are bombarding a virtual crystal to calculate the trajectories and slowing down of incident projectiles into matter and then to predict the expected backscattering events and spectra at various angles between the ion beam direction and the crystal axis. This step requires the description of the crystal model of apatite.

An idealized crystallographic model of fluorapatite was looked for and chosen from the literature to perform McChasy simulations in the subsequent task of determining the fraction of defects in both virgin and irradiated crystal samples. The apatite was modelled according to the well-established crystal structure of fluorapatite (hexagonal symmetry, space group P63m); lattice positions of major elements were set at known positions according to the literature (they were exactly fixed to their ideal positions) and trace elements (Th, La/Ce, and Y) were located at substitutional positions at Ca (1) or Ca (2) positions according to the most probable positions known for Durango's crystals, as established before in the literature and presented in table 2.4. Despite the fact that Durango's crystals embed a lot a different impurities in the structure, only a limited number were selected here, corresponding to the most abundant ones (La/Ce, Y and Th) since additionnal impurities that are present only at very low concentration have a negligeable role in the channelling phenomenon and therefore exhibit a neglieable contribution to the calculated backscattering spectra (both aligned and random). Such a simplication drastically reduces the calculation time for simulation with no loss of quality in terms of spectra quality.

Table 2.4

Matrix and trace elements utilized in crystal model of apatite for McChasy simulation. The lattice positions of matrix atoms are idealized positions, while the position for trace elements were inferred from the litterature. Positions are given assuming the P63m space group. Such a model was implemented into the McChasy code to define the apatite structure [49]

Matrix elements			
Atoms	X	Y	Z
Ca (1)	1/3	2/3	0
Ca (2)	5/26	1/13	¼
P	11/26	5/13	¼
O (1)	5/13	7/13	¼
O (2)	8/13	6/13	¼
O (3)	4/13	3/13	0
F	0	0	¼
Trace elements			
Atoms	X	Y	Z
Th	1/3	2/3	0
La	5/26	1/13	¼
Y	5/26	1/13	¼

In order to account for impurities and atomic positions, the chemical formula for fluorapatite, $Ca_5(PO_4)_3F$, was generalized to $A_5(BO_4)_3X$, with the cation A having two possible positions: A (1) and A (2) (Scheme 2.3). The model was created by putting the A (1) cations in the *b* layers and the A (2) and B cations in the *a* layers of ..*b*(*ab*)*a*.. packing of an HCP system. The A (1) cations form continuous isolated A (1) O6 trigonal prism columns parallel to *c* axis, as presented in Scheme 2.4, and these columns are linked through the BO_4 tetrahedra. A (2) cations from octahedra via A(2)O5X [50].

These octahedra, which are corner-connected to each other and to the A (1)O6 trigonal prisms, are cation-centered on the *b* anion nets, and form groupings of three, which are

joined at a common X atom at one of their apices. The A (2) octahedral parallel to (001) edge-share with the BO4 tetrahedra [50].

Scheme 2.3

Arrangement of cation-centered polyhedra in the idealized fluorapatite model. In the left side (I), the projection along [001] is shown while A(1)O6 , A(2)O5X, and BO4 connectivity were emphasized in the lower clinographic projections at the right side (II). Green: Fluorine, Red: Oxygen [50]

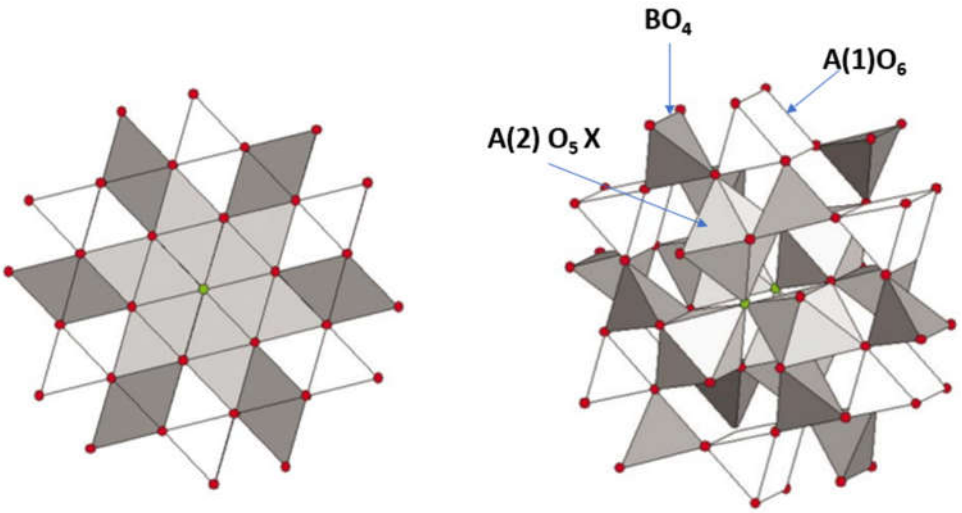

I II

Scheme 2.4

(a) The preferred topological representation of an idealized fluorapatite. A (1)O6 trigonal prisms/meta-prisms and the BO_4 tetrahedra were emphasized [50]. (b) Tetrahedral strings and c-axis repetition in a fluorapatite. Green: Oxygen [50]

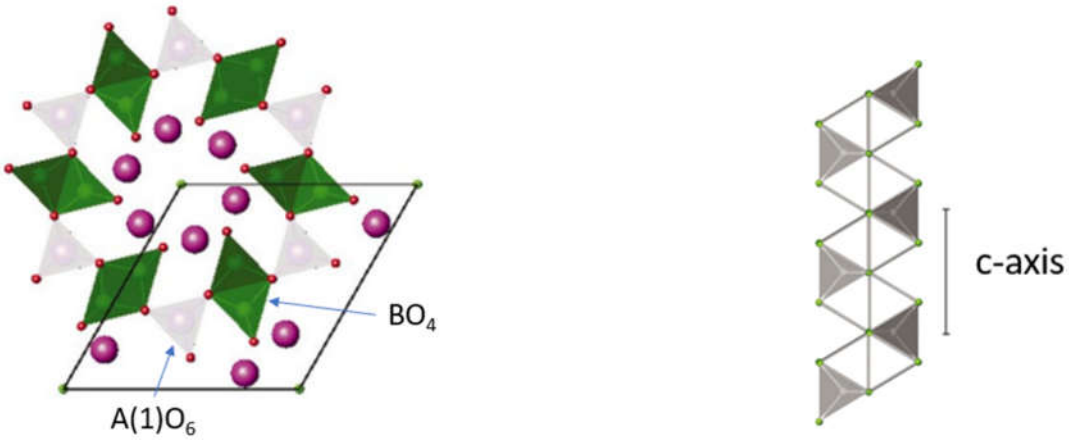

(a) (b)

2.5 Parameters related to ion beam and geometry of the experiment

The input file of simulation requires the definition of various parameters: geometry of the RBS/C experiment the scattering angle was constant at 165°, also about the incident particles (nature, energy was used for He^+ beam is 1.4 MeV, and the angular divergence of the beam fixed at 0.12°, such value corresponds to channeling measurements made on several crystals with different compositions in the past) and the channeling configuration along *c*-axis (Scheme 2.4.b) as defined by the crystal structure.

2.6 RBS Experiments: Data reduction

Spectra recorded from the first phase of experiments were analyzed and treated using the RUMP software to determine the crystal composition that is needed for subsequent McChasy simulations. As a matter of fact, a similar evaluation of the crystal composition can be achieved by the McChasy code but the RUMP software offers more flexibility for this task. McChasy code was used to determine the initial number of defects in the crystal assuming the ideal model for fluoroapatite, as described in section 2.4. The McChasy code was also used to study the evolution of radiation damage profile as a percentage of randomly displaced atoms (RDA) at various levels of alpha recoil nuclei fluence for the second phase of experiments, i.e., after the implantation treatment.

2.7 Monte Carlo simulations

The McChasy code was used to analyze the experimental RBS/C spectra. The operating concepts of the code are based on MC simulations. The McChasy code simulates the trajectory of light ions travel through crystals. According to independent depth profiles of various defect types, such as interstitials, edge dislocations, substitutions, stacking faults, or grain boundaries, the software provides a fitting procedure for RBS/C spectra, providing calculated channeling spectra as output. The code works well with heterostructures, superlattices, and materials with complex defects [51]. In the present case of our experimental investigation, the McChasy code simulation outputs were in good agreement with recorded spectra. In the present first approach of defect analysis, both individual random atomic displacements as well as severely distorted areas (atomic clusters) covering a few unit cells were modelled assuming the presence of RDA type defects. Defects that cause lattice distortions over tens of unit cells fall under the category of extended defects. Models of these defects include dislocations. In the McChasy code their shape follows an arctan function, in accordance with the Peierls-Nabarro theory [52].

The modelling of those more complex defects is complex and goes beyond the scope of the present investigation.

A trial-and-error fitting procedure has been performed out using the McChasy code:

The process begins with the creation of an input file that contains the thickness of a region of interest (usually the implanted part of a sample), divided into a number of slices, and an estimate of the concentration of defects in each slice for RDA. The program is then run for the specified number of incident ions. Following a comparison of the calculated and experimental spectra, the defect concentration may be changed to improve the fit. The simulation code is then run again using the updated input file. Until the ideal fit is found, the final stage is repeated. Examples of outputs of this simulation is shown in Figure 3.5 in Chapter Three.

2.8 The principle of TEM

The transmitted electrons which are the electrons passing through the sample before being collected, are what used in the transmission electron microscopy (TEM) method. The main advantage of electron microscopy is the capability to provide high resolution images of the defective structure of irradiated crystals and information regarding their structure (amorphous state for instance). Modern transmission electron microscopes can examine the position and chemistry of individual atoms [51]. For TEM (high vacuum), the typical pressure range for electron microscopes is 10^{-4} to 10^{-7} Pa [53]. TEM microscopes are primarily designed to test the specimen's internal structure because they generate highly focused beam of electrons which affect the specimen inside a vacuum chamber. The preferred method for analyzing specimen internal microstructure, evaluating nanostructures including particles, fibers, and thin films, and imaging atoms is transmission electron microscopy (TEM). The microstructural evolution of the irradiation apatite was observed using TEM on pre-implanted thin apatite foils in order to interpret the kinetics of damage buildup. Images were recorded by the microscopists at IJCLab and are not the topic of my research work.

Chapter Three

Results and Discussion

This section investigates the quality of the crystals before irradiation by the use of RBS and channeling experiments performed on the crystals. Also, it investigates the damage creation of heavy recoil nuclei in apatite and a possible recovery effect produced by the electronic stopping of probing ions. The results of this investigation are necessary in the experimental simulation of the accumulation of displacement damage caused by heavy recoil nuclei. The modeling of the crystal structure was discussed in the section 2.4.

This chapter discusses the simulation performed via Monte-Carlo McChasy code at room temperature, by implanting the crystals with 500 keV Bi^{3+} and the evaluation of the damage depth profile with the increase of ion fluence. In addition, results from TEM were collected to check the presence of crystal defects.

3.1 Crystal quality: qualification of samples

After the samples preparation was completed; eight crystals were obtained (one of the crystals was divided into two parts) and analysed by RBS and ion channelling using a goniometer. Then an irradiation step using 1.4 MeV He^{+} was done to put a well-defined charge Q of incoming particles at the crystal surface without inducing any significant radiation damage.

By continually rotating the goniometer (with an angle of 4° forming a cone around the major crystallographic direction of the sample) with respect to the major crystal axis [001] while performing out the RBS experiments, a random yield spectrum (the so-called random spectrum) for each of the samples was obtained. This random spectrum serves as a reference level of the backscattering yield that would be recorded on a polycrystalline sample of apatite. The main axis position (α, β) across the [001] direction for the ion channeling technique was then sought and the corresponding minimum axial yield (the so-called aligned spectrum) was recorded for the samples that were characterized in the first phase.

The ratio of aligned yield to random yield measured in an energy window just below the sample surface (the energy window from 700 to 770 keV, since it is the highest energy part of the spectrum) was measured from RBS/C experiments (Table 3.1) demonstrated

that five samples (Samples A, B, D, E, and F) are of high crystalline quality. Nevertheless, the comparison with the expected yield for an ideal crystal structure simulated with the McChasy code, suggests that the single crystal from Durango, Mexico may not be completely free of inclusions (there may be other phases and defects present) and/or that there may be a significant number of structural flaws, such as stacking faults, dislocations, and twins, which are present in naturally occurring fluorapatite and that were not totally removed by the annealing procedure. Nonetheless it is worth stressing that the theoretical minimum axial yield assumes an ideal structure of fluoroapatite as defined in Table 2.4 (see section 2.4) that is not the exact genuine structure of crystals naturally found: Thus, this theoretical value is clearly an underestimation of what can be obtained in reality even assuming a defect-free apatite sample. Table 3.1 below shows the absolute backscattering yield data for sample A, B, D, E and F, as measured at a depth just below the surface peak. Recorded minimal axial yields shows that the crystal quality is indeed very good: crystal D shows to the best of our knowledge the best ever recorded axial yield on a natural fluoroapatite single crystal.

A prepared sample should have an initial very low amount of native defects in order to perform a reliable irradiation test and a subsequent RBS/C experiment for radiation damage measurements. This requirement will increase sensitivity in measuring the subsequent damage evolution in a crystal, especially at very low irradiation fluences. The prepared carbon-coated samples' crystal quality was evaluated using a parameter called minimum axial yield, or χ_{min}. To choose crystals suitable for use in subsequent RBS/C experiments designed for damage buildup and damage annealing (recovery) research, the values of χ_{min} obtained for the different crystals were used. For the subsequent RBS/C experiments, crystals with χ_{min} values less than 0.15 were deemed suitable. Whereas the majority of natural apatite crystals have χ_{min} that is unsuitable for RBS/C experiments (typical χ_{min} larger than 0.3 up to 1 – such values are very common while preparing the crystals in a very careful way), excellent quality monocrystalline fluoroapatite crystals were obtained in the course of this work. Experimental minimum axial yield's minimum recorded value is as low as 0.085, where the minimum axial yield is defined as:

$$\chi_{min} = \frac{\text{Integral yield (counts) of the aligned}}{\text{Integral yield (counts) of the random}} \quad \ldots\ldots\ldots\ldots\ldots\ldots\ldots\ldots 3.1$$

Table 3.1

RBS absolute yields recorded at a shallow depth from the crystal surface for Sample A, B, D, E and F. The theoretical minimum yield corresponds to the expected value calculated by MC simulation assuming crystal atoms to be sited at their ideal positions given in Table 2.4.

Samples	Crystal Orientation	Integral Counts (*the energy window from 700 to 770)*	Aligned over Random Yield	Aligned over Random Yield, %	Typical Theoretical Minimum Yield
A	Aligned	20933	0.104	10.4%	
	Random	206094			
B	Aligned	13007	0.115	11.5%	
	Random	113097			
D	Aligned	17416	0.0845	8.45%	5.4%
	Random	205639			
E	Aligned	19328	0.0932	9.32%	
	Random	205826			
F	Aligned	20824	0.0981	9.81%	
	Random	21292			

The Aligned over Random Yield percent values shown in table 3.1 are far below 15% which indicate that the quality of the crystal is suitable for our work. The result for crystal D indicates that it has the best crystal quality at over a typical depth in the micrometer range as sensed by the probing ions.

Figure 3.1 below shows the plotted random and aligned yields for Sample D for qualitative reference.

Figure 3.1

Absolute RBS spectra recorded in random (blue signal) and aligned (gray signal) position (across the [001] direction) on sample D (spectra were obtained using 1.4 MeV He+ ions with a charge Q = 50 μC)

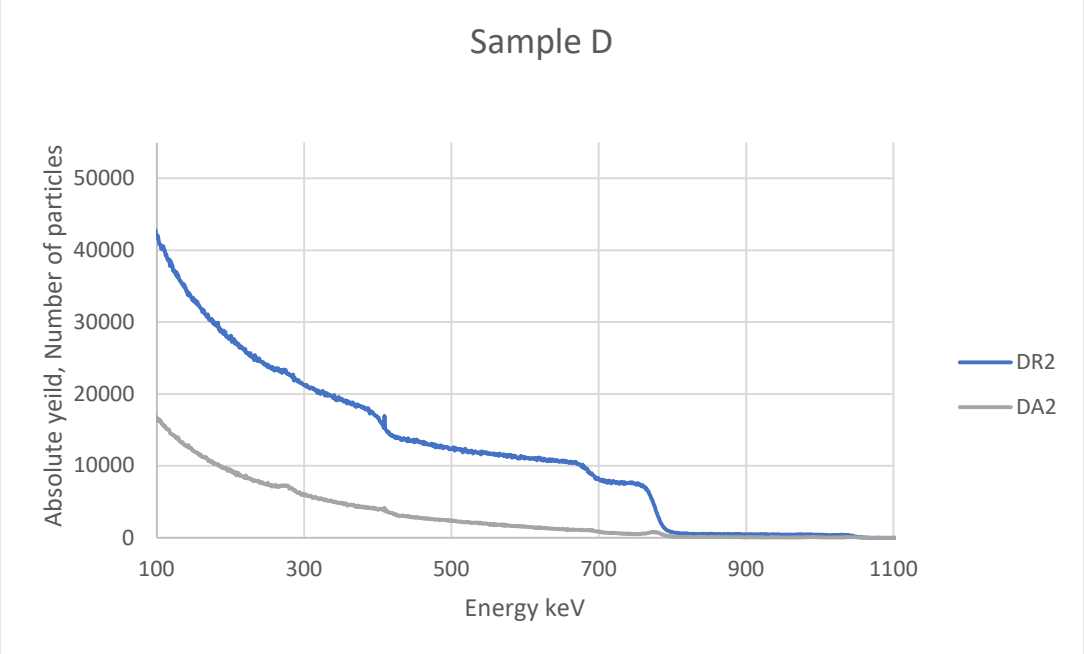

3.2 Analysis of natural fluorapatite crystal composition

The RUMP software was used to evaluate the composition of fluorapatite single crystals from Durango, Mexico using samples A, B, D, E, and F as experimental data. The backscattering yield in the random direction for each sample was plotted and several simulation runs were implemented to obtain a "simulation spectra" that will best fit in to the random spectra of the sample. This step was mandatory due to the presence of a lot of natural impurities in the Durango's crystals. Table 3.2 below shows the composition of the sample D based on the simulations that gave the best fit to the random spectra.

Table 3.2

Composition of the elements used in RUMP simulation that gave the best fit to the random spectra of fluorapatite. The theoretical atomic composition is $Ca_5(PO_4)_3F$. Fits were performed assuming the simplified model of apatite composition that contains a limited number of major foreign elements embedded into the structure

Element	Pure Apatite Form	Sample D
Ca	5	4.951
P	3	3
O	12	12
F	1	1
Th	0	0.002
La/Ce	0	0.034
Y	0	0.013

According to the simulation results in Table 3.2, the composition obtained for the sample D was found to be very similar to the pure apatite from Durango as investigated in former studies. A very small decrease in the calcium content of natural fluorapatite was observed as it was replaced by the three impurities. Such a result is in close agreement with investigations performed by various authors on the composition of apatite single crystals from Durango.

The experimental data from the goniometer for the five crystals is presented in Table (1) (see Appendix A). The simulation was achieved for the data for crystal D. Figure 3.2 shows the experimental and simulated spectra for comparison: it fits nicely with the random spectrum of sample D and enlightens the locations of the fronts for the various elements. A careful analysis of the experimental data shows that the natural apatite crystals contain impurities at trace levels that can be experimentally determined and quantified by RBS. Major impurities are light lanthanides (La and Ce that cannot be easily separated in the condition of the RBS analysis, since they have very similar masses and they are present here in small amounts only, due to the carbon layer deposited at the crystal surface), Y and a small contribution of Th. Figure 3.2 shows the best simulation spectrum to the experimental random spectrum of Sample D.

Figure 3.2

(a)Fluorapatite random spectrum (green stars) in comparison to the RUMP simulation spectrum (red line) for sample D. Arrows show the position of fronts corresponding to the various elements from both major (Ca, P, F, O) and trace elements (Ce, Y, Mn).(b) High energy region of the RBS spectrum (corresponding to the presence of trace elements) of the Durango natural apatite taken using 1.4 MeV He ions and scattering angle of 165°

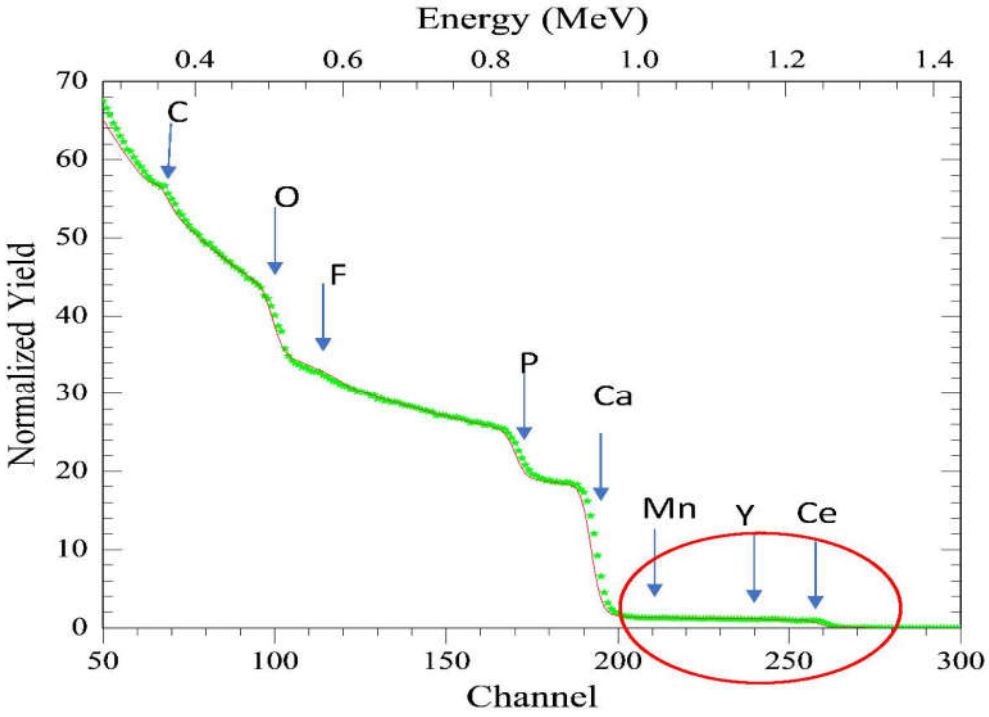

(a)

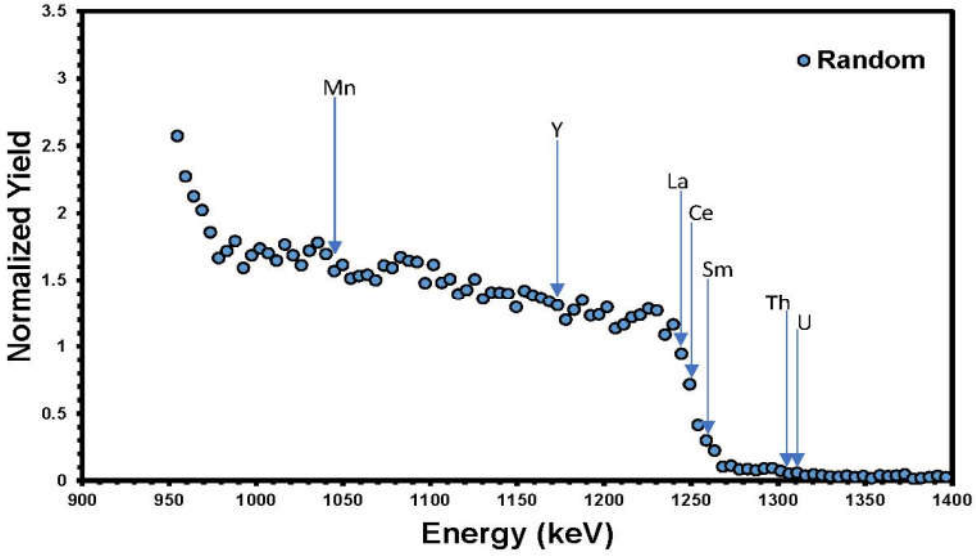

(b)

A zoom of the region representing the trace elements (located in the high energy part of the RBS signal) is show in Figure 3.2 (b). The expected positions of the fronts of the possible trace elements are indicated with their surface scattering energies. It can be clearly seen that the front located near 1250 keV can possibly be attributed to the presence of La, Ce, and Sm, while the very small front near 1300 keV can be ascribed to U, Th, and Pb.

A similar analysis as the one that was shown for the sample D was also conducted for other crystals. Figure 3.3 shows the corresponding aligned and random spectra plotted with the data collected on Table 1A (see Appendix A).

Figure 3.3

Random and aligned RBS spectra collected on various samples as a measurement test of their crystalline quality (Figure 3.3 is extracted from Table 1A Appendix A)

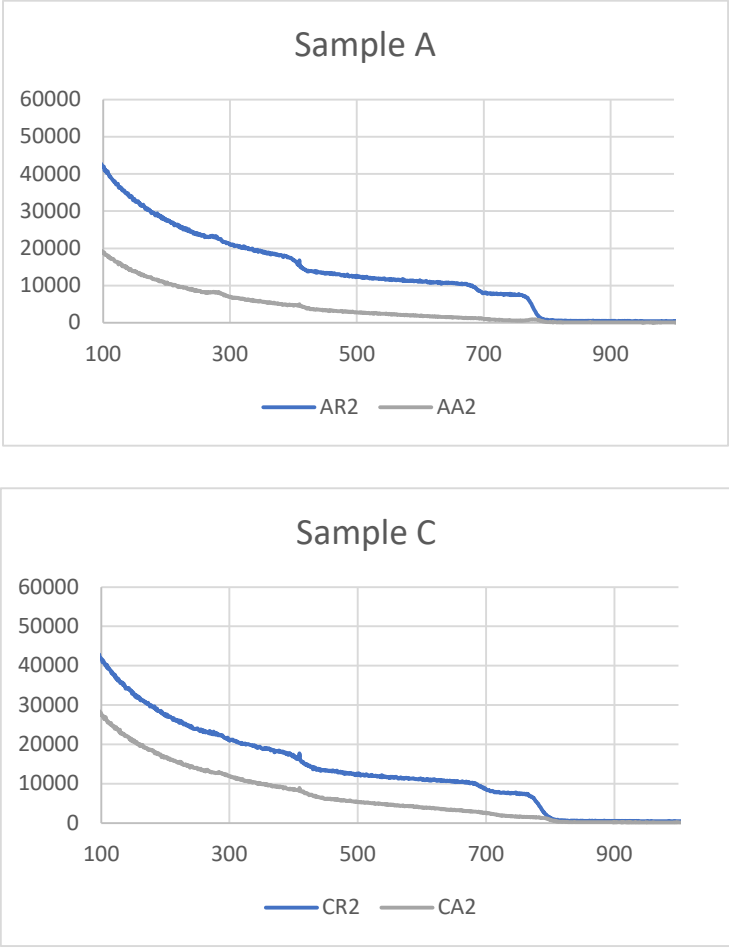

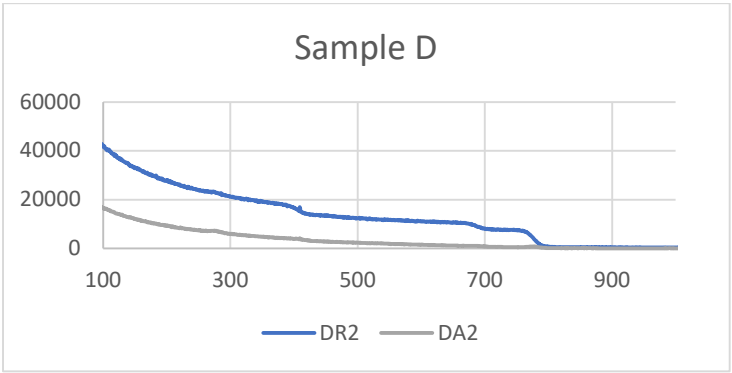

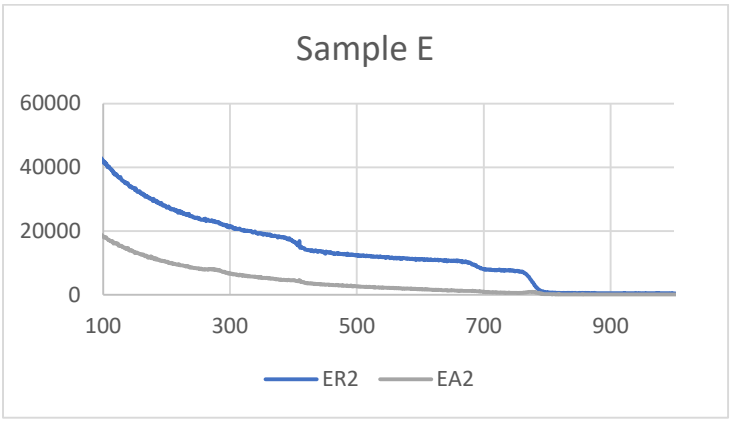

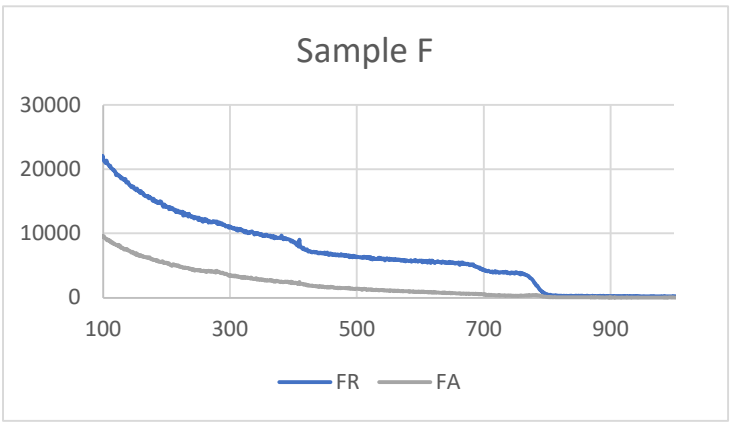

3.3 Native defects in fluorapatite

The McChasy code was used to calculate the quantity of natural defects in samples by comparison with the crystallographic model of fluorapatite described in the section 2.4 for ion channeling. The software takes into account the characterization parameters, such as energy calibration, projectile energy, geometry of the experiment (scattering angle) that were discussed in section 2.5.

In the simulation procedure, the crystal sample was divided into layers of a specific thickness, and for each layer, the fraction (percentage) of natural defects modeled by

randomly displaced atoms (RDA) was defined. RDA, which mimics every kind of defect that could exist in the structure in this first approach conducted here, is the apparent percentage of randomly displaced atoms produced by defects such as Frenkel pairs, extended defects, such as dislocations loops and lines, stacking faults, etc. In summary, we measured the contribution of all defects created by irradiation due to the sole contribution of obstruction-type using the RDA type of defect.

Since all defects are represented as pure RDA, the defect model is a simplification of the reality but it is known to correctly model the damage built-up in amorphisable solids. During the data analysis, we imposed that the amount of RDA employed in the simulations for a specific layer to be constant value for all atom types inside that layer, not only for specific atom specie that were present in that layer. Such an assumption was justified a posteriori since the disorder in all sublattices can be modelled with a satisfactory agreement.

Depending on how many projectiles were used for a single run of the simulation code, in order to collect a satisfactory statistic of events, the program was run, and a single simulation took from minutes to several hours to achieve completion. The output yield was then given for random and aligned spectra. A very large number of McChasy simulations were done until the simulation and experimental spectra reaches a good to very good agreement.

3.4 Simulation of RBS/C experimental spectra of apatite crystals irradiated at room temperature with 500 keV Bi ions

The damage level of crystals implanted at various Bi fluences were characterized using the backscattered He ions (see Scheme 3.1). In the first phase, the experiment involves the investigation of apatite crystals quality before pre-implantation as mentioned before in section 3.1. The second phase collects the result of the backscattered 1.4 MeV He^{+} ions for the apatite crystal implanted with 500 keV Bi^{3+} at different fluences, and the experimental data was obtained as shown below measures the damage that happened to the crystals by the analysis of the energy distribution (and thus depth distribution) of displaced atoms as shown by the evolution of aligned spectra plotted on Figure 3.4.

Scheme 3.1

Schematics of the RBS/C characterization of Bi pre-implanted crystals

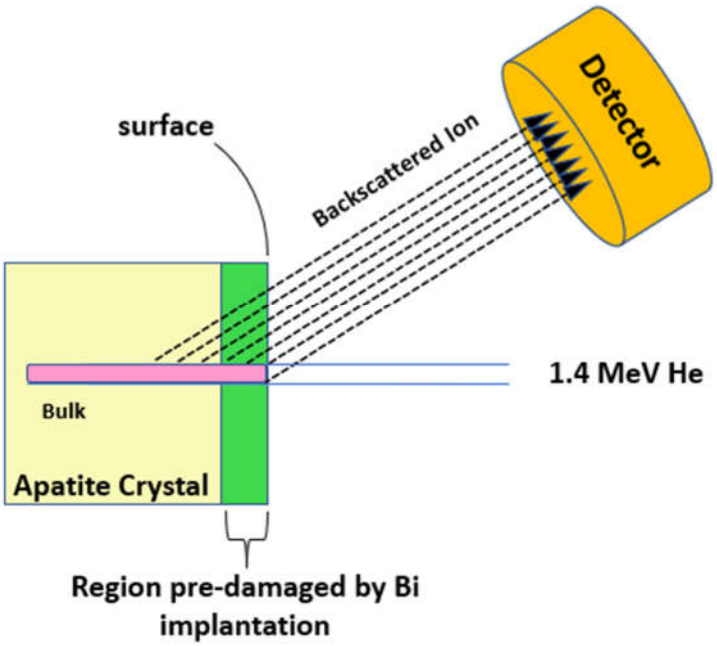

After completion of the crystal's characterization, all these experimental data were fitted to get information on the crystal evolution of 500 keV Bi^{3+} implanted apatite single crystals at room temperature.

3.4.1 Qualitative description of the crystal evolution.

The RBS/C experiments were performed on the apatite crystals at room temperature irradiated with 500 keV Bi ions at various ion fluence. The spectra in Figure 3.4 were extracted and plotted from the data in Table 2A in Appendix A. The comparison of the various random spectra recorded for the different samples show no difference before and after implantation. Such a result was anticipated because the amount of incorporated Bi atoms in crystals is too small to have a significant contribution to the RBS signals (in both random and aligned directions). The aligned spectrum recorded on the virgin sample shows a very good channeling behavior: a minimum axial yield and a low amount of native defect in the crystal. While increasing the ion fluence, we note the presence of a damaged peak that progressively grows: the peak is seen for all sublattices (it is best seen on the Ca and P sublattices) and demonstrates that part of matrix atoms are displaced with respect to their regular position in the crystal. For the upper fluence that was investigated, the aligned spectrum reaches the random level (see Figure 3.4) supporting the fact that a

very large amount of disorder was induced by irradiation in the crystal and that a possible amorphization was achieved.

Figure 3.4

RBS/C aligned and random spectra recorded on apatite crystals irradiated at room temperature with 500 keV Bi ions at various ion influences. The circles represent the spectra obtained from the characterization experiments

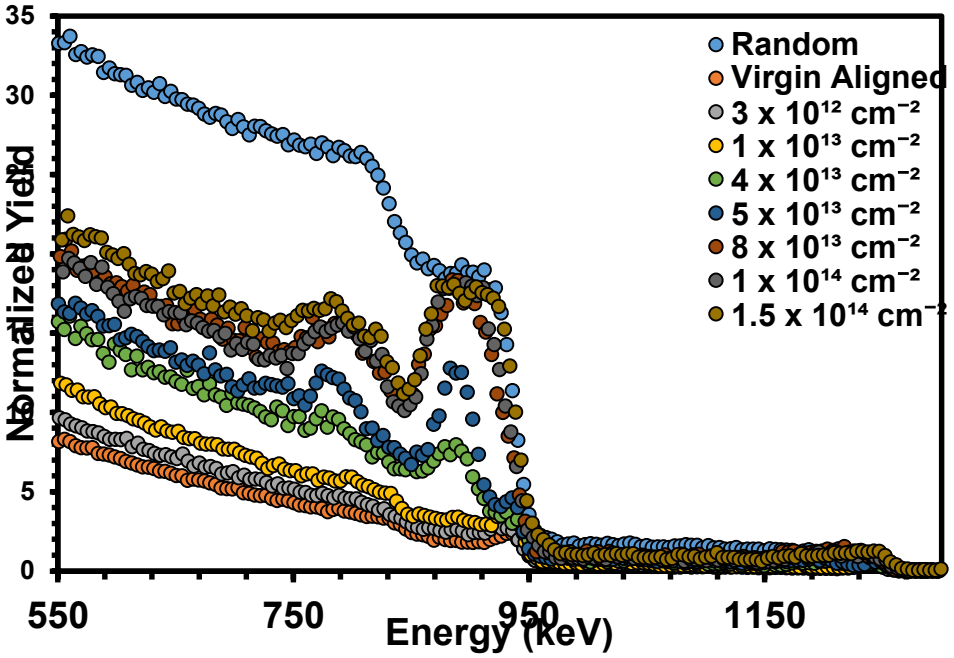

All the simulations were performed for experimental data at room temperature to do a comparison between the room temperature experiment and the irradiation experiment conducted at 100ºC. Indeed, due to the limited availability of the JANNuS-SCALP platform during the spring, some of the experiments are 100°C were not fully completed. Figure 3.5 shows the McChasy simulations of RBS/C experimental spectra of an apatite irradiated at room temperature with 500 keV Bi ions to various ion fluences. They are best fits to experimental spectra.

Figure 3.5

Monte Carlo simulation of RBS/C experimental spectra of apatite crystals irradiated at room temperature with 500 keV Bi ions at various ion influences. The circles represent the spectra obtained from the characterization experiments while the lines represent the best fits to the data obtained by simulation using the McChasy simulation code and the model of apatite crystal structure as described in section 2.4

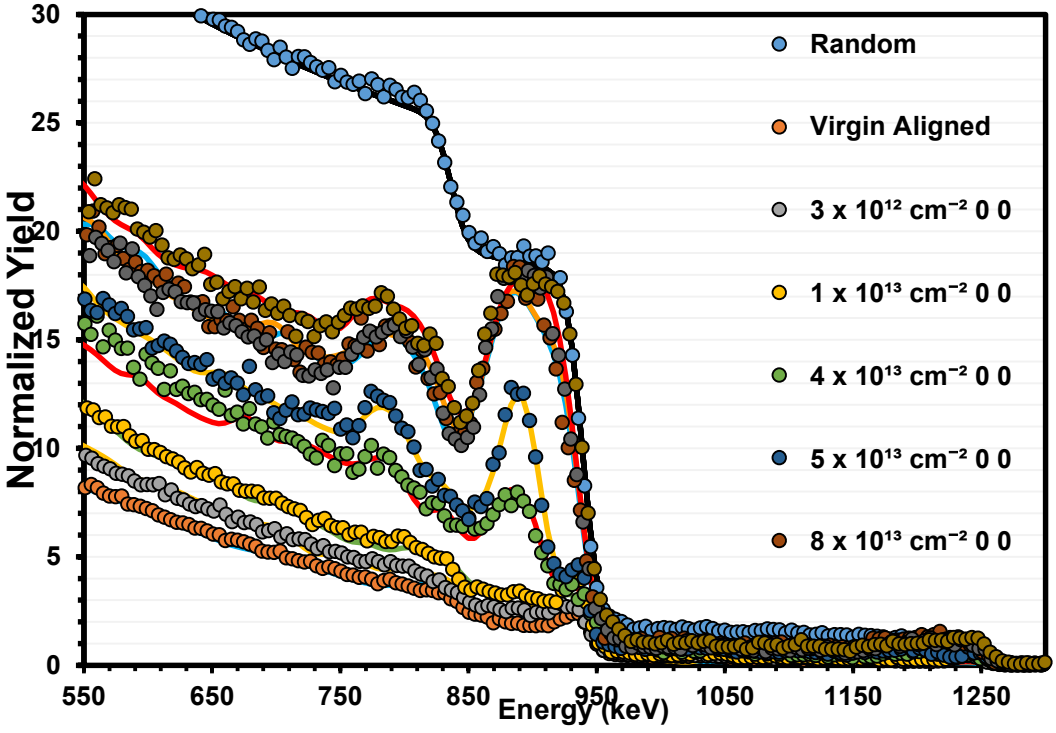

The McChasy code was applied to simulate the quantity of defects caused by alpha irradiation by modeling the disorder in terms of RDA using RBS spectra recorded at the fluences where a damage peak is clearly discernible and focusing mostly on the Ca sublattice since the sensitivity is the highest one (Ca is the heaviest matrix element). Figure 3.5 shows MC fits to experimental RBS spectra at increasing fluences: 3 x 10^{12} cm^{-2}, 1 x 10^{13} cm^{-2}, 4 x 10^{13} cm^{-2}, 5 x 10^{13} cm^{-2}, 8 x 10^{13} cm^{-2}, 1 x 10^{14} cm^{-2} and 1.5 x 10^{14} cm^{-2}. According to Figure 3.5, in the range of 10^{12} cm^{-2} no damage peak is visibly present for ion fluences, but the implanted Bi ions were still able to create some defects as seen by the small rise in the RBS/C yield in comparison to the virgin aligned spectra. At an ion fluence of 4 x 10^{13} cm^{-2}, a noticeable damage peak begins to appear for both the Ca (centered around 910 keV) and P sublattices (centered around 800 keV). The RBS/C yield grew quickly and a qualitative examination of the evolution of the spectra shows that most likely full amorphization from the crystal surface appears to have been reached at an ion fluence of 1.5 x 10^{14} cm^{-2}, while and a thin layer of an amorphized

region is already present at an ion fluence of 8 x 10^{13} cm^{-2}. Due to the displacement damage cascades caused by heavy ions impinging into the apatite crystals, which is known to cause amorphization in some materials, the evolution of the RBS/C spectra at this stage already shows clearly that amorphization is indeed very likely for the upper investigated fluences.

After several simulation runs, results from McChasy code simulations, as shown on Figure 3.5, are in good agreement with the experimental data collected from RBS experiments. It is worth stressing that the disorder induced by irradiation on both the Ca and the P sublattices are very well fitted at all fluence. Such a statement shows that the proposed model of defect that is based solely on RDA with the same amount of displaced atoms at a given depth for all sublattices is indeed able to correctly model the radiation-induced damage despite its apparent simplicity.

3.4.2 The evaluation of the damage-depth profile

Figure 3.6 (a) presented the evolution of the damage-depth profile with the increase of ion fluence, as extracted from the MC simulations. As shown in Figure 3.5, only a low amount of damage can be seen from the pristine crystal up to an ion fluence of 1x10^{13} cm^{-2}, but a regular increase of the disorder in the implanted region with the increase of ion fluence is evidenced. This damage is expected to be Frenkel pairs, small defect clusters or even small amorphous domains created by the displacement cascade (RBS/C alone cannot firmly conclude on the nature of defects: an in-depth investigation involving a charge in energy of the probing ions will provide more information, but such a study requires a lot of beam time and it is clearly beyond the scope of the present investigation). At an ion fluence of 4 x 10^{13} cm^{-2}, a wide damage zone at a depth extending from ~40 to ~120 nm starts to occur, corresponding to the fluence at which the presence of a damage peak can clearly be seen in the RBS/C spectra. At this damage state, it is likely that the amorphous domains have become more interconnected resulting to a damage layer possibly composed of crystalline material interlaced with amorphous domains. As the ion fluence increases as shown in Figure 3.6 (a), an increase in the width of the damage zone is observed until 100 % RDA is achieved from a depth of ~60 to ~75 nm at an ion fluence of 8 × 10^{13} cm^{-2}. This layer is very likely fully amorphous while the depth ranging from ~20 to ~40 and ~75 to 110 nm could contain extended defects or a mixture of fully damaged and partially damaged zones. A damage layer having 100% RDA is observed

from the surface up to a depth of 70 nm at an ion fluence of 1 x10^{14} cm^{-2}. This layer is assumed to be fully amorphous while the depth from ~70 to ~120 nm is only partially damaged. Also 100% RDA was observed from a depth ~40 to ~80 nm at an ion fluence of 1.5 x 10^{14} cm^{-2}. The maximum damge kinetic for each fluence was plotted against the percent RDA as shown in Figure 3.6 (b) which emphasizes the direct relationship between ion fluence the highest disorder

Figure 3.6

(a) Damage-depth profiles recorded on apatite crystals implanted with 500 keV Bi ions at room temperature. The damage levels are in units of %RDA which obtained by the use of the McChasy code to simulate RBS/C spectra for each ion fluence. The model assumes that all the damage can be reproduced by assuming that at a given depth a given fraction of lattice atoms is randomly displaced in the solid. (b) shows that as the ion fluence increases the damage in the apatite crystal increases

(a)

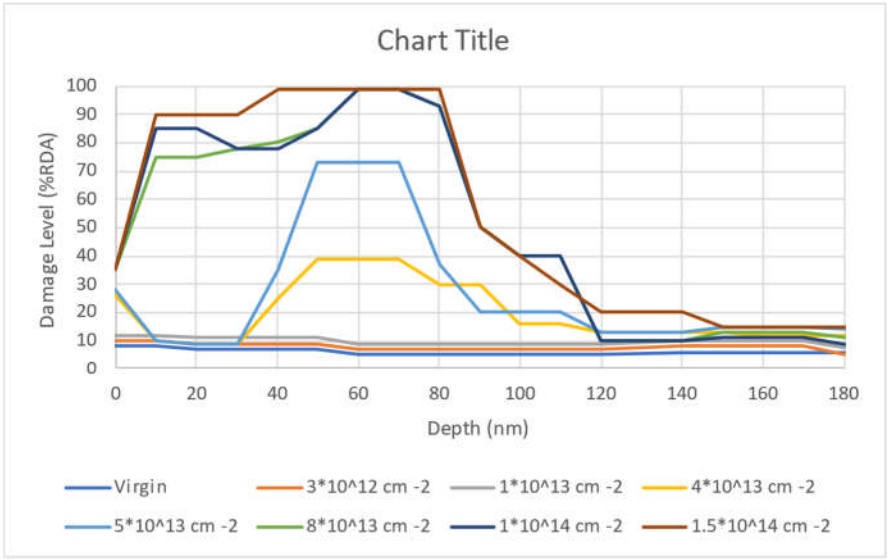

(b)

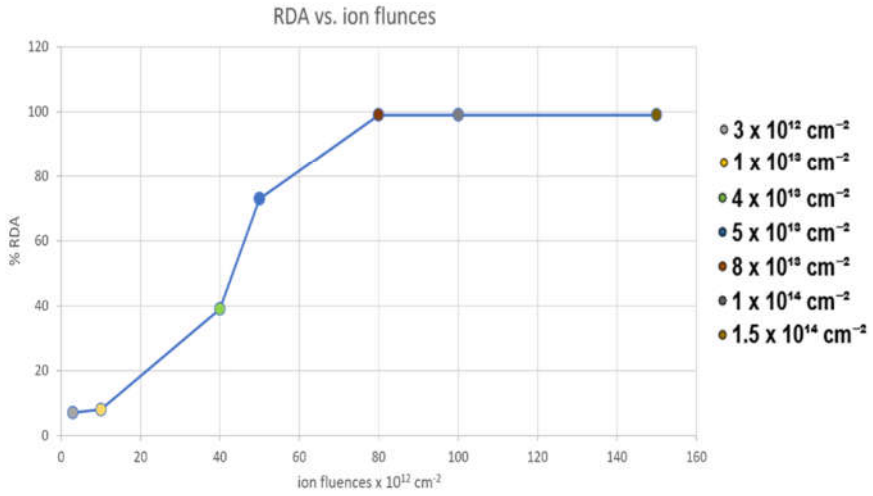

3.5 TEM Results

Further investigations on the behavior of fluorapatite crystals under irradiation was obtained using TEM analysis at various fluences.

TEM characterization utilized to represent a damage state that happened on the crystals at an ion fluence of 3 $x10^{12}$ cm^{-2}, so in this ion fluence no visible extended defects as shown in Figure 3.7 (a). The RDA depth distribution obtained from McChasy simulations is in good agreement with the damage zone seen on the TEM picture.

When a larger fluence was applied the TEM characterization reveals that a distinct damage layer starts to be observed at an ion fluence of 4 $x10^{13}$ cm^{-2} as presented in Figure 3.7 (b). The darker zone that appears in the image represent the extent of the damage inflicted on the crystal structure. In this damage state, the RDA depth distribution obtained from McChasy simulations is also in good agreement with the damage zone seen on the TEM image. The two edges of the damage band show strong strain contrasts (visible dark areas) which probably contains dislocations and defect clusters while the area between the edges only show few dark spots.

Using larger ion fluence, $1x10^{14}$ cm^{-2}, the domain of damage was increased as visibly appears in Figure 3.7 (c). And the RDA damage distribution is 100% at limited region. The RDA depth distribution obtained from McChasy simulations is matching with the damage zone seen on the TEM image. The edges of the amorphous layer remain crystalline which probably less ion impact occurs in this region. So, we conclude that when the ion fluences increase the damage also increases when applying various ion fluences.

Figure 3.7

TEM image recorded on an apatite single crystal irradiated at a fluences $3x10^{12}$ cm^{-2} , $4x10^{13}$ cm^{-2} , $1x10^{14}$ cm^{-2},respectively. This figure shows also the depth distribution of defects as measured by RBS/C (see previous section) and the depth distribution of Bi implanted ions calculated by the SRIM code

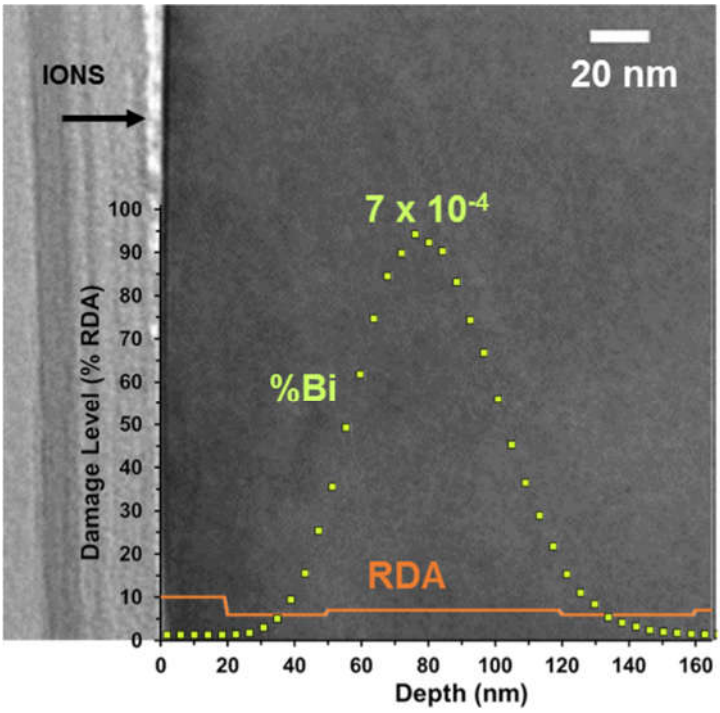

$3x10^{12}$ cm^{-2}

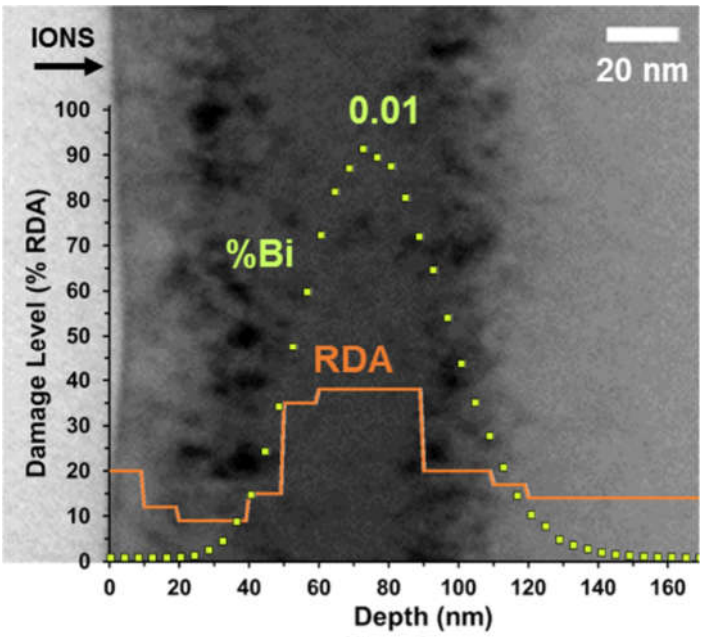

$4x10^{13}$ cm^{-2}

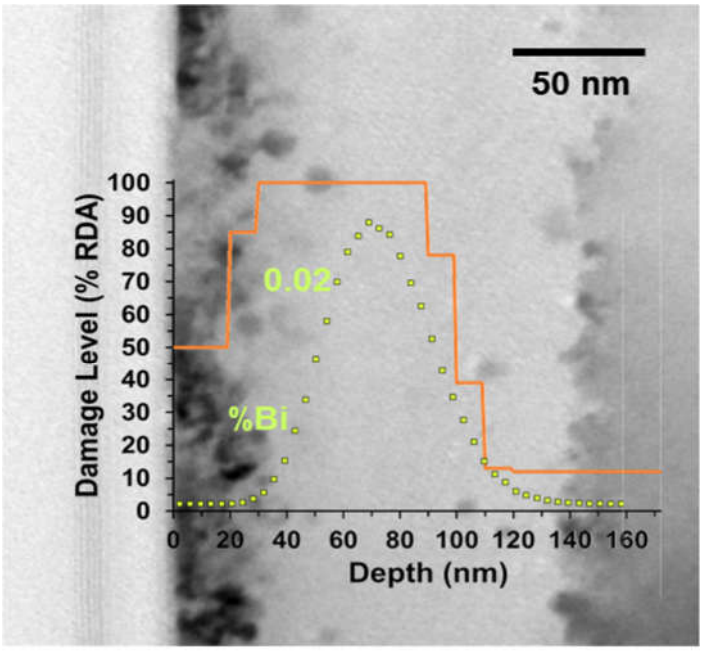

$1x10^{14}$ cm^{-2}

3.6 Conclusion

The effect of radiation, more precisely alpha decay of actinides, on the crystalline structure of natural fluoroapatite crystals $Ca_5(PO_4)_3F$ was studied using Bi^{3+} ions as a model of recoil nuclei. The ex-situ RBS/C technique was used to characterize 500 keV Bi implanted crystals at increasing ion fluence, simulating the effect of the damage generated by the heavy recoil nucleus. As the ion fluences increase the amount of damage which was modelled as RDA (Randomly Displaced Atoms) at all fluence increases and has greater effect in generating atomic displacements in natural fluorapatite. The Monte Carlo McChasy code simulation fits very satisfactorily the Rutherford Backscattering by channeling mode experimental results. TEM was utilized to characterize and observe induced defects for selected apatite samples which was pre-implanted with 500 keV Bi ions at room temperature at specific fluences where the damage kinetics shows a significant evolution. TEM characterization showed that the induced defects for the selected samples increase with increasing the ion fluence, in accordance with RBS/C results. The damage zone seen on the TEM images is also in good agreement with the RDA depth distribution obtained from McChasy simulations. An amorphous layer was observed at the large fluence in the range 10^{14} cm^{-2}, corresponding to the presence of a zone where a high RDA value was found.

3.7 Future perspective

1- Perform the implantation experiments at different temperatures.

2- Measure the optical density of the vacancy before and after implantation.

3- Study the stability of the crystal after implantation.

List of Abbreviations

Abbreviation	Meaning
(HLW)	High Level Waste
(ILW)	Intermediate Level Waste
(LLW)	Low Level Waste
(VLLW)	Very Low Level Waste
(IBA)	Ion Beam Analysis
(RBS)	Rutherford Backscattering Spectrometry
(RBS/C)	Rutherford Backscattering Spectrometry by Channeling mode
(RUMP)	Rutherford Universal Manipulation Program
(JANNuS)	Joint Accelerators for Nanoscience and Nuclear Simulation
(TEM)	Transmission Electron Microscope
(ERDA)	elastic recoil detection analysis
(PIXE)	particle-induced X-ray emission
McChasy	Monte Carlo Channeling Simulation code

References

1. Fuks, L., et al., *Methods of Thermal Treatment of Radioactive Waste.* Energies, 2022. **15**(1): p. 375.

2. Gin, S., et al., *An international initiative on long-term behavior of high-level nuclear waste glass.* Materials Today, 2013. **16**(6): p. 243-248.

3. Hyatt, N.C. and M.I. Ojovan, *Materials for nuclear waste immobilization*. 2019, MDPI. p. 3611.

4. Jay, E.E., *Atomistic scale modelling of phosphate mineral phases for nuclear waste form development.* 2012.

5. Coates, R., et al., *Managing Low Radioactivity Material from the Decommissioning of Nuclear Facilities*. 2008, IAEA, Technical Reports Series.

6. Lin, Z., et al., *Study on Irradiation Response of Nanocrystalline Phase in Sm-Doping Fluorapatite Glass-Ceramics under He Ion Irradiation.* Nanomaterials, 2022. **12**(7): p. 1194.

7. Jacoby, M., *As nuclear waste piles up, scientists seek the best long-term storage solutions.* Chemical & Engineering News, 2020. **30**.

8. Lennemann, W.L., *The management of high-level radioactive wastes.* IAEA Bull, 1978. **21**(4): p. 1-16.

9. Chaumont, J., et al., *Competition between disorder creation and annealing in fluoroapatite nuclear waste forms.* Journal of Nuclear Materials, 2002. **301**(2-3): p. 122-128.

10. Ewing, R.C., W.J. Weber, and F.W. Clinard Jr, *Radiation effects in nuclear waste forms for high-level radioactive waste.* Progress in nuclear energy, 1995. **29**(2): p. 63-127.

11. Bohre, A., K. Avasthi, and V.I. Pet'kov, *Vitreous and crystalline phosphate high level waste matrices: Present status and future challenges.* Journal of Industrial and Engineering Chemistry, 2017. **50**: p. 1-14.

12. Neumeier, S., et al., *New insights into phosphate based materials for the immobilisation of actinides.* Radiochimica acta, 2017. **105**(11): p. 961-984.

13. Jantzen, C. and M. Ojovan, *On selection of matrix (wasteform) material for higher activity nuclear waste immobilization.* Russian Journal of Inorganic Chemistry, 2019. **64**(13): p. 1611-1624.

14. Vance, E., B. Begg, and D. Gregg, *Immobilization of high-level radioactive waste and used nuclear fuel for safe disposal in geological repository systems*, in *Geological Repository Systems for Safe Disposal of Spent Nuclear Fuels and Radioactive Waste*. 2017, Elsevier. p. 269-295.

15. Vienna, J.D., *Nuclear waste vitrification in the United States: recent developments and future options.* International Journal of Applied Glass Science, 2010. **1**(3): p. 309-321.

16. McCloy, J.S. and S. Schuller, *Vitrification of wastes: from unwanted to controlled crystallization, a review.* Comptes Rendus. Géoscience, 2022. **354**(S1): p. 1-40.

17. Macerata, E., et al., *Immobilization of radioactive isotopes in fluorapatite matrices.* MRS Online Proceedings Library (OPL), 2009. **1193**.

18. Oelkers, E.H. and J.-M. Montel, *Phosphates and nuclear waste storage.* Elements, 2008. **4**(2): p. 113-116.

19. Haddad, Y., et al., *In situ characterization of irradiation-induced microstructural evolution in urania single crystals at 773 K.* Nuclear Instruments and Methods in Physics Research Section B: Beam Interactions with Materials and Atoms, 2018. **435**: p. 25-30.

20. Ouchani, S., J.-C. Dran, and J. Chaumont, *Evidence of ionization annealing upon helium-ion irradiation of pre-damaged fluorapatite.* Nuclear Instruments and Methods in Physics Research Section B: Beam Interactions with Materials and Atoms, 1997. **132**(3): p. 447-451.

21. Bar-Yosef Mayer, D.E. and N. Porat, *Green stone beads at the dawn of agriculture.* Proceedings of the National Academy of Sciences, 2008. **105**(25): p. 8548-8551.

22. Zhou, S., et al., *Preparation and characterization of phosphate glass–ceramic wasteform with strontium fluoride.* Journal of Radioanalytical and Nuclear Chemistry, 2021. **328**(1): p. 217-224.

23. Rigali, M.J., P.V. Brady, and R.C. Moore, *Radionuclide removal by apatite.* American Mineralogist, 2016. **101**(12): p. 2611-2619.

24. Metcalfe, B.L., et al., *Ageing of a phosphate ceramic used to immobilize chloride contaminated actinide waste.* Journal of nuclear materials, 2009. **385**(2): p. 485-488.

25. *National Center for Biotechnology Information (2022). PubChem Compound Summary for CID 10207414, Fluorapatite. Retrieved December 16, 2022 from https://pubchem.ncbi.nlm.nih.gov/compound/Fluorapatite.* 2022; Available from: https://pubchem.ncbi.nlm.nih.gov/compound/Fluorapatite.

26. Macerata, E., et al., *Fluorapatite as immobilization matrix for nuclear waste.* Radiation Effects and Defects in Solids, 2018. **173**(9-10): p. 763-771.

27. Cui, W., et al., *Adsorption behaviors of different water structures on the fluorapatite (001) surface: a DFT study.* Frontiers in Materials, 2020. **7**: p. 47.

28. Wang, J., *Incorporation of iodine into apatite structure: a crystal chemistry approach using Artificial Neural Network.* Frontiers in Earth Science, 2015. **3**: p. 20.

29. Soulet, S., *Etude des effets d'auto-irradiation dans des matériaux à structure apatitique*. 2000, Université Paris Sud-Paris XI.

30. Ewing, R.C. and L. Wang, *Phosphates as nuclear waste forms.* Reviews in mineralogy and geochemistry, 2002. **48**(1): p. 673-699.

31. Ault, A.K., C. Gautheron, and G.E. King, *Innovations in (U–Th)/He, fission track, and trapped charge thermochronometry with applications to earthquakes, weathering, surface-mantle connections, and the growth and decay of mountains.* Tectonics, 2019. **38**(11): p. 3705-3739.

32. Mansour, S., et al., *Combined Zircon/Apatite U-Pb and Fission-Track Dating by LA-ICP-MS and Its Geological Applications: An Example from the Egyptian Younger Granites.* Minerals, 2021. **11**(12): p. 1341.

33. Miro, S., *Study of damage and helium diffusion in fluoro-apatites*. 2004, Caen Univ. Basse-Normandie.

34. Djimbi, D.M., et al., *Impact of apatite chemical composition on (U-Th)/He thermochronometry: An atomistic point of view.* Geochimica et Cosmochimica Acta, 2015. **167**: p. 162-176.

35. *https://energyeducation.ca/encyclopedia/Alpha_decay Alpha decay.* 2022.

36. Weber, W.J., et al., *Radiation effects in crystalline ceramics for the immobilization of high-level nuclear waste and plutonium.* Journal of Materials Research, 1998. **13**(6): p. 1434-1484.

37. Mayer, M. *Rutherford backscattering spectrometry (RBS)*. in *Workshop on Nuclear Data for Science and Technology: Materials Analysis*. 2003.

38. Perrière, J., *Rutherford backscattering spectrometry.* Vacuum, 1987. **37**(5-6): p. 429-432.

39. Rubin, S., T. Passell, and L. Bailey, *Chemical analysis of surfaces by nuclear methods.* Analytical Chemistry, 1957. **29**(5): p. 736-743.

40. *https://sites.google.com/a/lbl.gov/rbs-lab/ion-beam-analysis/ion-channaling Ion Channeling*. [cited 2018; Available from: https://sites.google.com/a/lbl.gov/rbs-lab/ion-beam-analysis/ion-channaling.

41. Mamalakis, E., *Data Analysis of RBS Spectra using Differential Evolution.* 2019.

42. Kolodzey, J., et al., *Electrical conduction and dielectric breakdown in aluminum oxide insulators on silicon.* IEEE Transactions on Electron Devices, 2000. **47**(1): p. 121-128.

43. Berling, D., et al., *FexNi100− x nanometric films deposited by laser ablation on SiO2/Si substrates.* Applied surface science, 2007. **253**(15): p. 6522-6526.

44. Cho, B., et al., *Ion beam analysis of pigments.* MRS Online Proceedings Library, 1990. **185**(1): p. 125-132.

45. Umapathy, G., et al. *Composition profile of thin film target by Rutherford backscattering Spectrometry*. in *Proceedings of the 61st DAE-BRNS Symposium on Nuclear Physics, Kolkata, India*. 2016.

46. Jóźwik, P., et al., *Analysis of crystal lattice deformation by ion channeling.* Acta Physica Polonica A, 2013. **123**(5): p. 828-830.

47. Gao, J., et al., *Ion-irradiation induced dislocation loops formation in high purity Co-free High Entropy Alloys.* Thursday 21st of January: p. 14.

48. Garrido, F. *https://www.in2p3.cnrs.fr/sites/institut_in2p3/files/page/2020-04/8-Doc-GARRIDO.pdf*. 2020; Available from: https://www.in2p3.cnrs.fr/sites/institut_in2p3/files/page/2020-04/8-Doc-GARRIDO.pdf.

49. Luo, Y., et al., *Crystal chemistry of Th in fluorapatite.* American Mineralogist, 2011. **96**(1): p. 23-33.

50. White, T. and Z. Dong, *Structural derivation and crystal chemistry of apatites.* Acta Crystallographica Section B: Structural Science, 2003. **59**(1): p. 1-16.

51. Jozwik, P., et al., *Advanced Monte Carlo Simulations for Ion-Channeling Studies of Complex Defects in Crystals.* Theory and Simulation in Physics for Materials Applications: Cutting-Edge Techniques in Theoretical and Computational Materials Science, 2020. **296**: p. 133.

52. Turos, A., et al., *Mechanism of damage buildup in ion bombarded ZnO.* Acta Materialia, 2017. **134**: p. 249-256.

53. Inkson, B.J., *Scanning electron microscopy (SEM) and transmission electron microscopy (TEM) for materials characterization*, in *Materials characterization using nondestructive evaluation (NDE) methods*. 2016, Elsevier. p. 17-43.

Appendices

Appendix A

Important tables

Table 1A

Data appear from the goniometer for different crystals

AO	AP	AQ	AR	AS	AT	AU	AV	AW	AX	AY	AZ	BA	BB	BC	BD	BE	BF	BG	BH
Channel	Grouped	Channel	Grouped	Channel	Grouped	Channel	Grouped	Channel	Grouped	Channel	Grouped	Channel	Grouped	Channel	Grouped	Channel	Grouped	Channel	Grouped
1	0	1	2	1	2	1	1	1	7	1	8	1	8	1	10	1	1	1	3
2	1	2	6	2	1	2	0	2	7	2	7	2	5	2	16	2	2	2	1
3	0	3	8	3	3	3	1	3	16	3	4	3	9	3	13	3	5	3	2
4	7	4	10	4	19	4	3	4	18	4	7	4	28	4	13	4	7	4	7
5	13	5	19	5	29	5	16	5	45	5	17	5	28	5	19	5	18	5	7
6	37	6	43	6	65	6	40	6	128	6	50	6	37	6	48	6	50	6	10
7	37	7	82	7	161	7	105	7	261	7	112	7	201	7	117	7	118	7	52
8	316	8	202	8	446	8	290	8	600	8	261	8	482	8	264	8	274	8	138
9	846	9	524	9	1167	9	739	9	1461	9	608	9	1271	9	632	9	705	9	314
10	2428	10	1524	10	3197	10	2114	10	3768	10	1643	10	3206	10	1625	10	1766	10	802
11	6897	11	3978	11	7876	11	5729	11	8996	11	3962	11	8310	11	4283	11	4472	11	2118
12	17994	12	9956	12	18739	12	14242	12	21051	12	9183	12	19540	12	9788	12	10033	12	4845
13	40138	13	21138	13	39548	13	30632	13	42686	13	18913	13	40513	13	20326	13	20887	13	9975
14	74385	14	38536	14	70633	14	54361	14	75694	14	33666	14	72583	14	36149	14	36503	14	17674
15	1E+05	15	57395	15	1E+05	15	81048	15	1E+05	15	49874	15	1E+05	15	54450	15	55355	15	27051
16	2E+05	16	74088	16	1E+05	16	1E+05	16	1E+05	16	64803	16	1E+05	16	70476	16	73797	16	35230
17	2E+05	17	84802	17	2E+05	17	1E+05	17	2E+05	17	74019	17	2E+05	17	81232	17	86009	17	41051
18	2E+05	18	89145	18	2E+05	18	1E+05	18	2E+05	18	78034	18	2E+05	18	85982	18	93138	18	43619
19	2E+05	19	89726	19	2E+05	19	1E+05	19	2E+05	19	79121	19	2E+05	19	87458	19	97071	19	44859
20	2E+05	20	88364	20	2E+05	20	1E+05	20	2E+05	20	78806	20	2E+05	20	86074	20	96666	20	44173
21	2E+05	21	86187	21	2E+05	21	1E+05	21	2E+05	21	76138	21	2E+05	21	84289	21	95218	21	43477
22	2E+05	22	83967	22	2E+05	22	1E+05	22	2E+05	22	73716	22	2E+05	22	81842	22	93390	22	42372
23	2E+05	23	81472	23	2E+05	23	1E+05	23	2E+05	23	71586	23	2E+05	23	79113	23	91984	23	41353
24	2E+05	24	78913	24	2E+05	24	1E+05	24	2E+05	24	69391	24	2E+05	24	76693	24	89651	24	39551
25	2E+05	25	76739	25	2E+05	25	1E+05	25	2E+05	25	67353	25	2E+05	25	74603	25	87764	25	38502
26	2E+05	26	74785	26	2E+05	26	1E+05	26	2E+05	26	65731	26	2E+05	26	72289	26	85265	26	37703
27	2E+05	27	72594	27	2E+05	27	1E+05	27	2E+05	27	64409	27	2E+05	27	70952	27	84185	27	36351
28	2E+05	28	70601	28	2E+05	28	1E+05	28	2E+05	28	62660	28	2E+05	28	68371	28	82311	28	35596
29	2E+05	29	68875	29	2E+05	29	1E+05	29	2E+05	29	60709	29	2E+05	29	66936	29	80434	29	34432
30	2E+05	30	67023	30	2E+05	30	99031	30	2E+05	30	59168	30	2E+05	30	64724	30	78978	30	33474
31	1E+05	31	65542	31	1E+05	31	97223	31	2E+05	31	57351	31	1E+05	31	64132	31	76651	31	32925
32	1E+05	32	63859	32	1E+05	32	95392	32	1E+05	32	56050	32	1E+05	32	61662	32	75761	32	32244
33	1E+05	33	62007	33	1E+05	33	92793	33	1E+05	33	54938	33	1E+05	33	60513	33	74426	33	31086
34	1E+05	34	60744	34	1E+05	34	90939	34	1E+05	34	53213	34	1E+05	34	58917	34	73546	34	30143
35	1E+05	35	59137	35	1E+05	35	88971	35	1E+05	35	51795	35	1E+05	35	57968	35	71898	35	29380
36	1E+05	36	57378	36	1E+05	36	87813	36	1E+05	36	51204	36	1E+05	36	55910	36	70313	36	29110
37	1E+05	37	56210	37	1E+05	37	85450	37	1E+05	37	50048	37	1E+05	37	55194	37	69106	37	28353
38	1E+05	38	55465	38	1E+05	38	83781	38	1E+05	38	48494	38	1E+05	38	53338	38	68067	38	27555
39	1E+05	39	54130	39	1E+05	39	82403	39	1E+05	39	47472	39	1E+05	39	52597	39	67229	39	26937
40	1E+05	40	52763	40	1E+05	40	80490	40	1E+05	40	46522	40	1E+05	40	51258	40	66188	40	26342
41	1E+05	41	51705	41	1E+05	41	78905	41	1E+05	41	45238	41	1E+05	41	50473	41	65230	41	25826
42	1E+05	42	50573	42	1E+05	42	78271	42	1E+05	42	44789	42	1E+05	42	48973	42	63632	42	25428
43	1E+05	43	49621	43	1E+05	43	76496	43	1E+05	43	43453	43	1E+05	43	47895	43	63228	43	25067
44	1E+05	44	49152	44	1E+05	44	74896	44	1E+05	44	42570	44	1E+05	44	47169	44	62228	44	24637
45	1E+05	45	47642	45	1E+05	45	74366	45	1E+05	45	41507	45	1E+05	45	46167	45	61329	45	23878
46	1E+05	46	46825	46	1E+05	46	72830	46	1E+05	46	40967	46	1E+05	46	45291	46	60226	46	23495
47	1E+05	47	46208	47	1E+05	47	71243	47	1E+05	47	40001	47	1E+05	47	44282	47	59421	47	22932
48	1E+05	48	44772	48	1E+05	48	70169	48	1E+05	48	39093	48	1E+05	48	43060	48	59568	48	22507
49	1E+05	49	44283	49	1E+05	49	68683	49	1E+05	49	38694	49	1E+05	49	42533	49	57637	49	22255
50	1E+05	50	43166	50	1E+05	50	67538	50	1E+05	50	37849	50	1E+05	50	41840	50	57410	50	21727
51	1E+05	51	42495	51	1E+05	51	66886	51	1E+05	51	37190	51	1E+05	51	40814	51	56532	51	21477
52	1E+05	52	41699	52	1E+05	52	65400	52	1E+05	52	36264	52	1E+05	52	39952	52	55738	52	20712
53	1E+05	53	40817	53	1E+05	53	64370	53	1E+05	53	35601	53	1E+05	53	39128	53	55246	53	20441
54	1E+05	54	40339	54	1E+05	54	63488	54	1E+05	54	34676	54	1E+05	54	38397	54	54356	54	20235
55	1E+05	55	39222	55	1E+05	55	62259	55	1E+05	55	33889	55	1E+05	55	37905	55	53596	55	19932
56	1E+05	56	38799	56	1E+05	56	61871	56	1E+05	56	33669	56	1E+05	56	37114	56	53248	56	19335
57	1E+05	57	38310	57	1E+05	57	60560	57	1E+05	57	33130	57	1E+05	57	36810	57	52896	57	18829
58	1E+05	58	37918	58	1E+05	58	59333	58	1E+05	58	32216	58	1E+05	58	35957	58	51779	58	18744
59	39593	59	36601	59	39670	59	58746	59	1E+05	59	31867	59	1E+05	59	35525	59	51563	59	18483
60	38379	60	36134	60	38613	60	57628	60	39091	60	31528	60	38842	60	34398	60	50821	60	18004
61	37174	61	35560	61	37104	61	57454	61	38018	61	30732	61	37692	61	33872	61	50170	61	17633
62	36069	62	34812	62	35855	62	56321	62	37039	62	30203	62	36618	62	33505	62	49398	62	17217
63	35356	63	34512	63	35898	63	55579	63	36088	63	29967	63	36237	63	33111	63	49291	63	17203
64	34606	64	33825	64	34461	64	55127	64	34991	64	29360	64	34597	64	32418	64	48718	64	16959
65	34103	65	33168	65	33972	65	53876	65	34327	65	28964	65	34311	65	31994	65	48147	65	16756
66	32607	66	32646	66	32975	66	53353	66	33647	66	28835	66	34202	66	31859	66	48516	66	16445
67	32469	67	32690	67	32305	67	53478	67	33449	67	28687	67	33582	67	31840	67	47473	67	16575

Table 2A

Experimental data at room temperature for implanted with 500 keV Bi^{3+} ion

Appendix B

Important figures

Figure 1B

Apatite Structure ($A_{10}(BO_4)_6X_2$), projected onto the (001) plane. The thin dashed blue lines highlight the unit cell (hexagon lattice shown here as a diamond shape). Red spheres are oxygen, light blue polyhedrons are Ca (I) cations, the light blue spheres are Ca (II) cations, the green spheres are channel anions (X), the purple tetrahedrons are B site cations. The thin light blue lines highlight bond0s[28]

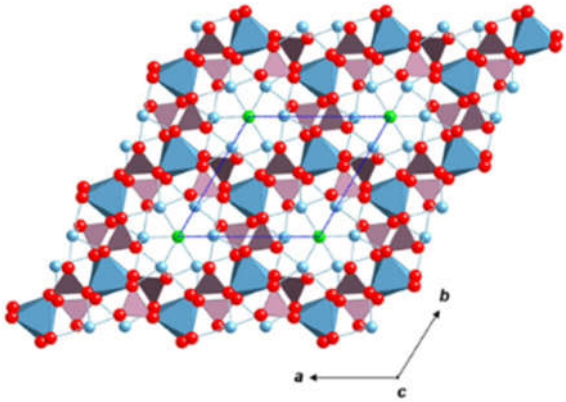

Figure 2B

Picture of one crystal from two large single crystals studied during the internship. Both crystals came from Mexico Durango location

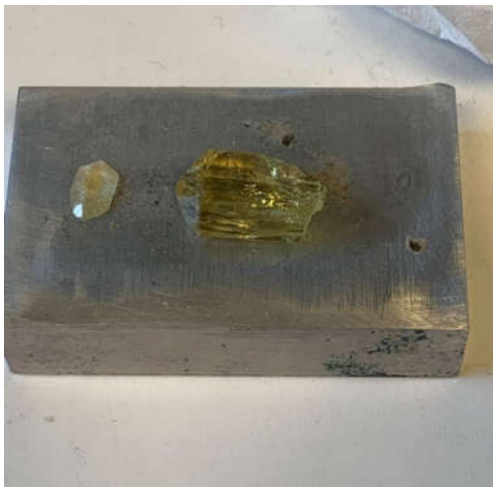

Figure 3B

Schematic picture of the JANNuS-Orsay Irradiation Platform, showing the 2-MV tandem accelerator, the 190 kV ion implanter and the various beam lines

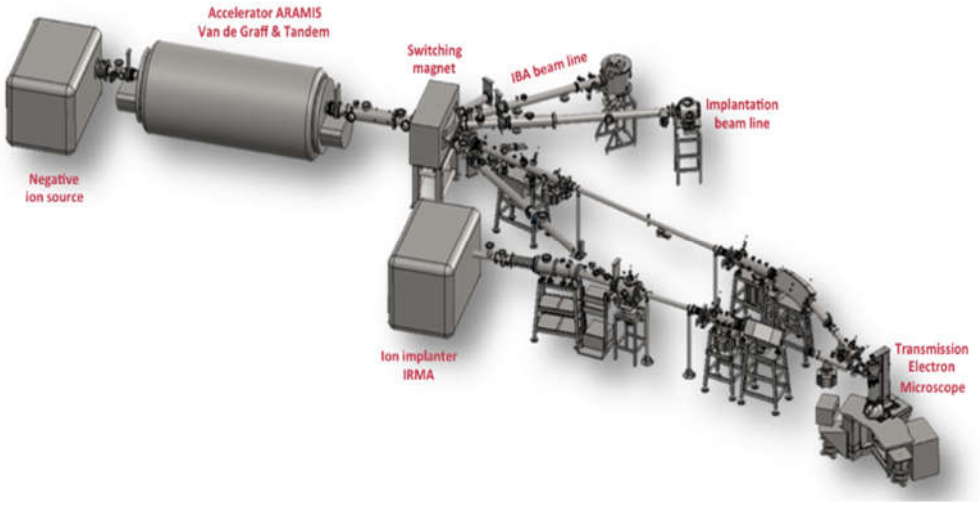

Figure 4B

Aluminum sample holder containing nine samples (crystal slices). The first six slices (from A to F) are from the same crystal chunk of apatite that was cut and the final three (G, H1, H2) from the second crystal. Note that some of crystals still show the hexagonal symmetry at macroscopic scale

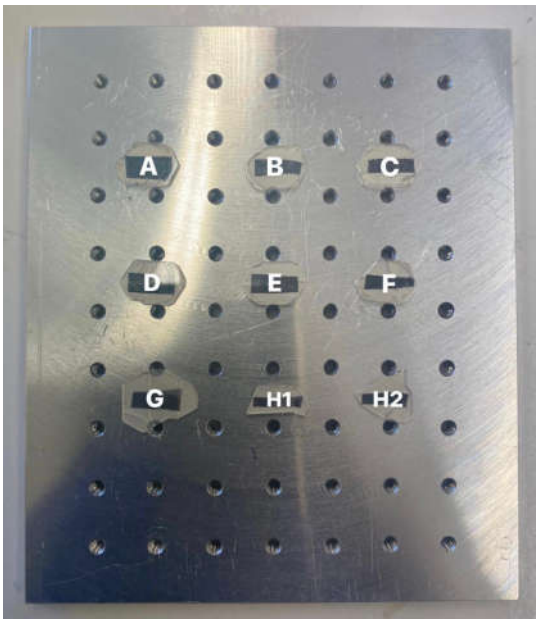

Appendix C

Machines used in this work

Figure 1C

Crystal cutting set-up using a diamond edge saw machine. The single crystal was placed on the designated sample holder while the diamond wire was placed perpendicular to the [001] direction of the crystal. A rotation machine is responsible in moving the wire which cut the crystal into slices

Figure 2C

Fluorapatite crystal (2-mm thick) glued on a polishing sample holder (1) and a mechanical polishing set-up using a disk polisher (2). A small quantity of diamond solution and water were sprayed to the cloth paper. Crystal was then pressed and lightly rub against the surface while the disk is rotating. The friction caused by the rotating disk polished the crystal surface due to the presence of diamonds having well-defined dimensions

(1)

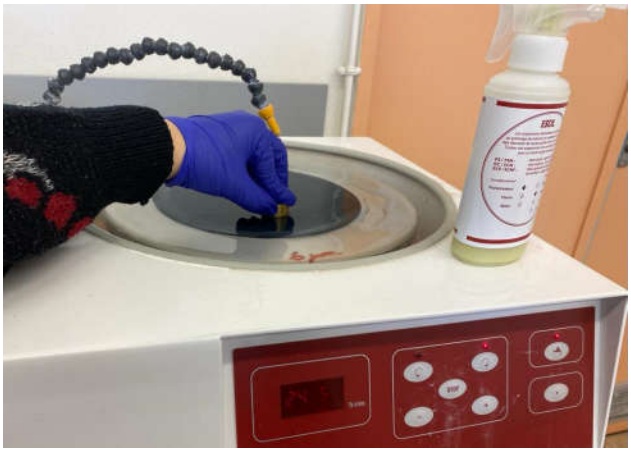

(2)

Figure 3C

High-temperature furnace used to anneal apatite crystals at temperature 900°C for 24 hours under air. This treatment is used to remove the structural damage caused by polishing step and restore the crystalline structure

Figure 4C

Carbon coater machine (Cressington carbon coater) used to deposit a graphite layer on one of the face polished of the crystals

جـامعـــة النجاح الوطنية

كليـــة الدراســـات العليـــا

استقصاء السلوك الإشعاعي لبلورات الفلورو أباتيت كمصفوفات لتجميد النفايات النووية

إعداد

رند غسان حزّام

إشراف

د. محمد سليمان

أ.د. فريدريكو جاريدو

قدمت هذه الرسالة استكمالا لمتطلبات الحصول على درجة الماجستير في الكيمياء، من كلية الدراسات العليا، في جامعة النجاح الوطنية، نابلس- فلسطين.

2023

استقصاء السلوك الإشعاعي لبلورات الفلورو أباتيت كمصفوفات لتجميد النفايات النووية

اعداد

رند غسان حزّام

إشراف

د. محمد سليمان

أ.د. فريدريكو جاريدو

الملخص

يمثل التوليد المتزايد للنفايات المشعة من التطبيقات الاقتصادية والعناصر المشعة تحديًا كبيرًا من حيث التخلص الآمن والتخزين. تم اقتراح بلورات الفلورابايتيت كحل محتمل لتجميد النفايات النووية بسبب قدرتها على تكوين مصفوفة صلبة وغير قابلة للذوبان يمكن أن تحتوي بشكل فعال على عناصر مشعة. ومع ذلك ، باعتبارها تقنية جديدة نسبيًا ، يلزم إجراء مزيد من البحث لتقييم فعاليتها وسلامتها على المدى الطويل بشكل كامل.

الهدف: يهدف هذا البحث إلى فهم تأثير الإشعاع الناجم عن تحلل الأكتينيدات في بلورات الفلورابايتيت ($Ca_5(PO_4)_3F$) ، والتحقيق في العيوب البلورية في الأباتيت الطبيعي ومعدلات الشفاء. بالإضافة إلى ذلك ، فإنه يهدف إلى تحديد ما إذا كان يمكن استخدام الأباتيت كمصفوفة بديلة محتملة لتضمين النفايات المشعة عالية المستوى (HLW) ، مثل منتجات الانشطار والأكتينيدات الثانوية ، المخزنة حاليًا في النظارات النووية.

الطريقة: تم استخدام تقنية غرس الأيونات بتجربة ex – situ، حيث تم زرع بلورات فلوروابايتيت الطبيعية المحضرة مسبقًا ($Ca_5(PO_4)_3F$) ، والتي تم الحصول عليها من منجم دورانجو في المكسيك ، باستخدام 500 كيلو إلكترون فولت من Bi^{3+} (أيونات ثقيلة) في منشأة JANNuS الواقعة في IJCLab لمحاكاة تحلل الأكتينيدات. تم تطبيق موائع مختلفة تتراوح من 10^{12} إلى 10^{14} سم$^{-2}$ في درجات حرارة مختلفة خاصة عند درجة حرارة الغرفة وعند 100 درجة مئوية. تم بعد ذلك توصيف العينات باستخدام التحليل الطيفي / توجيه

رذرفورد الخلفي للتشتت الخلفي (RBS/C) على خط شعاع تحليل الشعاع الأيوني (IBA) للمنصة باستخدام أيونات He^{+} 1.4 MeV في ظروف التوجيه. تمت محاكاة بيانات أطياف RBS باستخدام محاكاة مونت كارلو McChasy كود (RBS/C). يسمح هذا النهج المعتمد بإجراء تحليل شامل للخصائص الهيكلية والتركيبية لبلورات الأباتيت قبل وبعد التشعيع ، مما يوفر نظرة ثاقبة لتأثيرات نوى الارتداد الثقيل ومحاكاة تحلل الأكتينيد. تم استخدام المجهر الإلكتروني للإرسال (TEM) لمراقبة تطور الضرر الناجم عن أيونات Bi^{3+}.

النتائج: أظهرت بيانات أطياف RBS التي تمت محاكاتها باستخدام محاكاة مونت كارلو McChasy كود تشكيل الضرر في البلورة الناجم عن القذف بأيونات Bi^{3+}، بتأثيرات مختلفة. تم استخلاص توزيع الضرر وحركياته من تجارب RBS / C ومقارنتها بصور المجهر الإلكتروني النافذ (TEM) لمراقبة تطور الضرر الناجم عن أيونات Bi^{3+}، والتي استنتجت وجود مناطق غير متبلورة في بلورات الأباتيت المفردة ، مما يدعم الفكرة الرئيسية يمكن استخدام الأباتيت كمصفوفة بديلة لتضمين HLW.

الاستنتاجات: تمت دراسة تأثير إشعاع تسوس ألفا للأكتينيدات على التركيب البلوري لبلورات الفلورلباتيت الطبيعية ($Ca_5(PO_4)_3F$) باستخدام أيونات Bi^{3+} كنموذج لنواة الارتداد. تم استخدام تقنية RBS/C ex− situ لتوصيف البلورات المزروعة بواسطة 500 keV Bi^{3+} في زيادة تدفق الأيونات ، ومحاكاة تأثير الضرر الناتج عن نوى الارتداد الثقيل. تتلاءم محاكاة مونت كارلو McChasy كود بشكل مرضٍ للغاية مع تشتت رذرفورد العكسي عن طريق توجيه النتائج التجريبية للوضع. نظرًا لأن زيادة تركيز الأيونات تزيد من مقدار الضرر الذي تم تصميمه على أنه RDA (ذرات مزاحة عشوائيًا) حتى التغيّر النهائي للبلورة في نطاق 10^{14} سم$^{-2}$. أظهر توصيف TEM أن العيوب المستحثة لعينات الأباتيت المختارة تزداد مع زيادة تأثير الأيونات ، وهذا يتوافق مع نتائج RBS/C.

الكلمات الرئيسية: بلورات فلورو أباتيت ؛ مطيافية / توجيه رذرفورد العكسي (RBS/C) ؛ RBS/C ex – situ ؛ محاكاة مونتي كارلو McChasy كود ؛ نفايات عالية المستوى (HLW) ؛ أيونات Bi^{3+}.